

A robust autoassociative memory with coupled networks of Kuramoto-type oscillators

Daniel Heger and Katharina Krischer*
*Physics Department, Technical University of Munich,
 85748 Garching, James-Frank-Str. 1, Germany*

Uncertain recognition success, unfavorable scaling of connection complexity or dependence on complex external input impair the usefulness of current oscillatory neural networks for pattern recognition or restrict technical realizations to small networks. We propose a new network architecture of coupled oscillators for pattern recognition which shows none of the mentioned flaws. Furthermore we illustrate the recognition process with simulation results and analyze the new dynamics analytically: Possible output patterns are isolated attractors of the system. Additionally, simple criteria for recognition success are derived from a lower bound on the basins of attraction.

I. INTRODUCTION

Synchronization of oscillators, i.e., "the adjustment of rhythms due to an interaction" [1], is a ubiquitous concept representing one mechanism leading to collective dynamics. Its occurrence spreads over all scientific disciplines, with applications in engineering, physics, chemistry, biology, medicine and even in social sciences. The study of synchronization behavior has been correspondingly intense during the last two to three decades, the state of the art being summarized in recent textbooks, monographs and focus issues [1–8].

A particularly intriguing area where synchronization often occurs is neuroscience. The synchronization of neural oscillators controls vital functions but is responsible for neural diseases as well. Synchronization phenomena are also involved in cognition tasks of the brain [9]. The wish to understand and mimic information processing of the brain led to a separate field called computational neuroscience. Concomitantly, novel types of hardware were proposed that mimic some aspects of neural information processing. Their massively parallel operation is inherently different from the operating modes of all types of processors in everyday hardware. In this manuscript, we discuss a novel coupling scheme for oscillators that generates synchronization patterns and thus can be used as an autoassociative memory.

When an *autoassociative memory* is presented with a defective and/or incomplete piece of data, it recognizes and retrieves the correct data from a set of correct candidates. From a different point of view, the defective input data are mapped onto the most similar of the candidates. The ability to "map" is also found in complex physical systems: The trajectory of a system state will converge to an attractor. If several attractors exist, different sets of initial conditions, called *basins of attraction*, will end up on different attractors. Therefore, the system "maps" all initial conditions within one basin onto its attractor. Note that few physical systems are actually suitable as autoassociative memories: First, suitable mappings of the defective data onto the initial conditions and from

the attractors back onto the correct patterns have to be found. Additionally, initial conditions as well as attractors of a system need to be controlled, with the latter usually being difficult. Finally, the initial defective data should be mapped onto the most similar correct data candidate, which requires that the basins of attraction actually conform with a sensible definition of similarity. The idea to use basins of attractions for pattern recognition has originally been proposed by Hopfield for use in neural networks [10]. Contributions from mathematics, physics and neuroscience (see the end of [11] for a summary) made it possible to merge his ideas with the studies of coupled nonlinear oscillators.

Networks of nonlinear oscillators have been shown to act as autoassociative memory devices for binary patterns [12–19] according to the above-mentioned principle. In the original architecture [12–14], identical Kuramoto oscillators [11] are fully interconnected via programmable connections that can change sign and strength of the coupling according to the Hebbian Rule [20]. If the dynamics are expressed in phase shifts, fixed points are the only type of attractors, and defective input patterns as well as correct pattern candidates can be mapped on two synchronized groups of oscillators whose phases differ by π .

However, this design has two disadvantages:

- No distinct, well-separated fixed points exist for the memorized patterns [21]. Instead, there is one global attractor consisting of lines of attractive fixed points with neutrally stable eigendirections that connect every memorized pattern with every other. On short timescales, pattern recognition still works: Starting at the defective pattern, the system state quickly relaxes onto the global attractor close to the most similar pattern. On the attractor, however, perturbations due to external noise or implementation inaccuracies dominate and the system state drifts away from the correct pattern on longer timescales. Additionally, recognition success cannot be guaranteed as no well-defined basin of attraction exists for any single output pattern.
- The number of connections scales quadratically with the number of oscillators, so no large networks can be implemented in hardware.

* Contact: daniel.heger@ph.tum.de and krischer@ph.tum.de

So far, no architecture that solves both issues has been proposed. However, separate solutions for each problem have been discussed: Nishikawa et al. [18] showed that the degeneracy of the attractor can be lifted by adding second order Fourier modes to the coupling. A similar network with third order Fourier modes has been proposed as well [19]. A partial solution for the scaling problem has been proposed by Hoppensteadt and Izhikevich [15] and has been further advanced by Hölzel and Krischer [16] and Kostorz et al. [17]: Oscillators of different frequencies are coupled to the same global coupling that affects every oscillator differently. These architectures require an external input of complex time-dependent functions, but the number of connections scales with $\mathcal{O}(N)$.

Here, we propose an architecture that combines isolated attractors and minimal scaling of connection complexity without the need for complex external input. To this end, we built on previous studies [15, 16] of globally coupled oscillatory devices, but we introduce two peculiar features: Different temporal modulation of the coupling strength and a replacement of the single network by two interconnected subnetworks. The result is a robust autoassociative memory that is straightforward to be implemented as hardware and can be readily read out. Additionally, we can predict recognition success analytically. Thus, by exploiting the mutual interaction of two sub-networks, we arrive at a network architecture with superior functionality.

In the next section, the structure of our new architecture is described in detail. Afterwards, we obtain the effective dynamics through averaging, analyze its fixed points and derive the error-free capacity in Sec. III. In order to predict recognition success, Sec. IV derives a lower bound on the basins of attraction. The resulting criterion for guaranteed matching is then validated with simulations of the full dynamics in Sec. V. Before results are summarized in Sec. VII, Sec. VI compares the architecture to previous autoassociative networks of oscillators.

II. A NEW SCALABLE ARCHITECTURE

The proposed architecture consists of two identical networks of N oscillators each with equal frequency distribution. Oscillators within each of these "subnetworks" are globally coupled and the coupling strength is additionally modulated in time. For the first network, the coupling modulation [22] is constructed from products of signals of the second network's oscillators and vice versa. Due to its symmetrical layout, which is visualized in Fig. 1, we name the network the MONACO-Architecture: *Mirrored Oscillator Networks for Autoassociative COmputation*.

Motivated by experiments with networks of electrical Van-der-Pol-oscillators [16, 17], we assume that the oscillators are weakly coupled in one variable, have sinusoidal signals and a phase response curve proportional to a co-

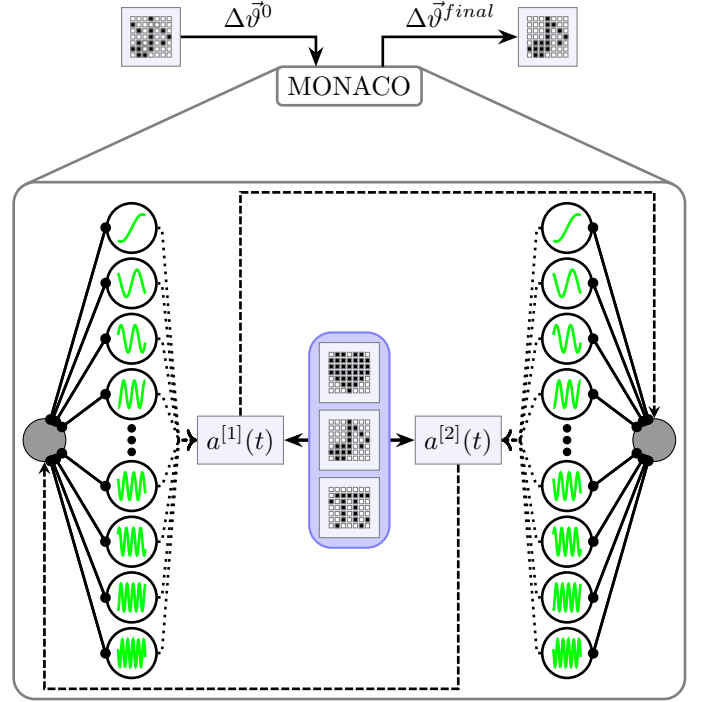


FIG. 1: Schematics of our new MONACO-Architecture: Oscillators (depicted as black circles surrounding a green sine-wave) are divided into two networks with the same frequency distribution that are both globally coupled. Coupling strength of both global couplings is modulated in time with functions $a^{[1]}(t)$ / $a^{[2]}(t)$ that depend on physical signals of oscillators from the other network and patterns shown in the middle.

sine. Then, the recognition dynamics can be reduced to a phase description [23]:

$$\begin{aligned}
 \dot{\vartheta}_i^{[1]} &= \Omega_i + \cos \vartheta_i^{[1]} \cdot a^{[2]}(t) \cdot \frac{\epsilon}{N} \sum_{j=1}^N \sin \vartheta_j^{[1]} \\
 \dot{\vartheta}_i^{[2]} &= \Omega_i + \cos \vartheta_i^{[2]} \cdot a^{[1]}(t) \cdot \frac{\epsilon}{N} \sum_{j=1}^N \sin \vartheta_j^{[2]} \\
 a^{[1]}(t) &= \sum_{k,l=1}^N S_{kl} \sin \vartheta_k^{[1]} \sin \vartheta_l^{[1]} \\
 a^{[2]}(t) &= \sum_{k,l=1}^N S_{kl} \sin \vartheta_k^{[2]} \sin \vartheta_l^{[2]}
 \end{aligned} \tag{1}$$

$\vartheta_i^{[1]}$ is the phase of the i -th oscillator in the first network and Ω_i its natural frequency. In the global signal $a^{[2]}(t) \cdot \epsilon/N \cdot \sum_{j=1}^N \sin \vartheta_j^{[1]}$, $a^{[2]}(t)$ denotes the coupling modulation generated from the second network's signals and ϵ is a small parameter which will be shown to be the effective coupling strength of the averaged dynamics. The amplitude perturbation is converted into a change in phase by multiplying with the phase response function

$\cos \vartheta_i^{[1]}$ and the coupling matrix \mathbf{S} controls attractors of the system.

Note that the frequency distribution is the same in both networks, so N pairs of oscillators with equal frequency exist. For sufficiently weak coupling and specifically chosen frequencies, S_{ij} only effectively connects oscillator pairs i and j and the architecture can act as an autoassociative memory: Apart from $\Omega_i \neq \Omega_j \forall i \neq j$, all frequencies Ω_i must be larger than $\Omega_{max}/3$ and all difference frequencies $\Delta\Omega_{ij} = \Omega_i - \Omega_j$ must be pairwise different as shown in Appendix A. As we demonstrate below (Eq. (5)), these conditions allow for further simplification of Eq. 1.

As the oscillator pairs of equal frequency synchronize at phase differences $\Delta\vartheta_i = \vartheta_i^{[1]} - \vartheta_i^{[2]}$ of either 0 or π ($\pm 2\pi$) in this setup, the $\Delta\vartheta_i$ are easy to read out (e.g. with one signal multiplication and a low-pass filter) and will be our "system state" to be manipulated. The coupling matrix is chosen according to the Hebbian Rule [20]:

$$S_{ij} = \sum_{m=1}^M \alpha_i^m \alpha_j^m \text{ with } \alpha_i \in \{\pm 1\} \quad (2)$$

Then attractors will exist for each memorized pattern $\vec{\alpha}^m$ and its inverse $-\vec{\alpha}^m$ according to the following $\{\Delta\vec{\vartheta} \mapsto \vec{\alpha}\}$ -mapping (see also Sec. III):

$$\begin{aligned} 0 + 2\pi n &\mapsto +1 \\ \pi + 2\pi n &\mapsto -1 \end{aligned} \quad (3)$$

When we talk about patterns "being attractive", it is meant in the sense that attractors in $\Delta\vec{\vartheta}$ exist according to this mapping.

Assume a defective pattern $\vec{\alpha}^d$ should be recognized as a pattern $\vec{\alpha}^{m'}$, which is the most similar to $\vec{\alpha}^d$ out of M correct pattern candidates $\vec{\alpha}^m$. For the recognition, $\vec{\alpha}^d$ is set as initial condition of the network according to Eq. (3) and the coupling matrix S_{ij} contains all correct pattern candidates as memorized patterns according to Eq. (2). As the defective pattern is close to the correct pattern in phase space, the system state will move to an attractor representing $\vec{\alpha}^{m'}$ and can be read out. Note that setting initial conditions is fast and easy in the MONACO-architecture: As the system state is coded into phase differences, simply coupling oscillator pairs with negative or positive sign according to $\Delta\vartheta_i = -\alpha_i^d \cdot E \sin \Delta\vartheta_i$ and $E \gg \epsilon$ for a short time $T_{init} \ll 1/\epsilon$ ensures a correct initialization.

If instead of an erroneous pattern only a small correct part of a pattern is known, missing pixel in $\vec{\alpha}^d$ can be filled with $+1$ or -1 with equal probability. Afterwards, recognition is performed as above.

Phase differences $\Delta\vartheta_j$ from an exemplary simulation of the phase dynamics (Eq. (1)) are shown in Fig. 3 for $N = 49$ oscillator pairs and 6 defective pixels. The memorized patterns $\vec{\alpha}^m$ used are visualized in Fig. 2 and are not orthogonal in the sense that $\langle \vec{\alpha}^{m_1}, \vec{\alpha}^{m_2} \rangle \neq 0$

$\forall m_1, m_2$ and $m_1 \neq m_2$ (\langle, \rangle denotes the standard scalar product.). The erroneous phase differences change to represent the correct \blacklozenge -shaped output pattern.

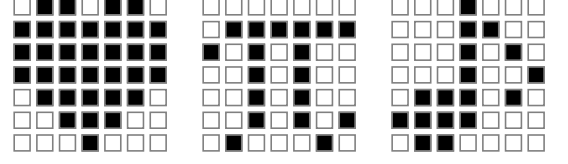


FIG. 2: Non-orthogonal patterns with 49 pixels that were used as memorized patterns $\vec{\alpha}^m$ in simulations for Fig. 3, Fig. 4 and the statistics in Sec. IV. $\alpha_i^m = +1$ is visualized as a black pixel and white pixels correspond to $\alpha_i^m = -1$.

However, the recognition process can fail if the number of erroneous pixels is too large. A failed recognition is shown in Fig. 4: The system state moves to an unknown attractor which corresponds to none of the $\vec{\alpha}^m$. In order to predict recognition success, a simple criterion is derived and tested in Sec. IV.

Before analyzing the dynamics, we want to point out that the coupling matrix \mathbf{S} does not need to be wired explicitly, which would require $\mathcal{O}(N^2)$ connections. By rewriting both coupling modulations as squares of scalar products instead, they can be generated with $\mathcal{O}(N \cdot M)$

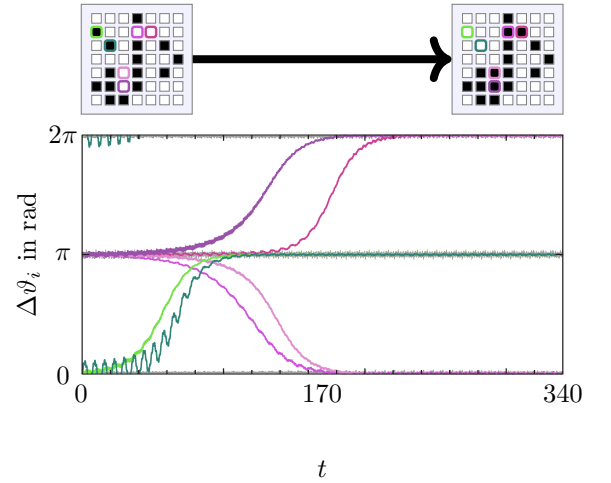


FIG. 3: Successful Recognition: A binary pattern with 6 erroneous pixels (colored and thick) shown on the top left is correctly recognized as one of 3 memorized patterns shown in Fig. 2. White pixels are mapped onto $\Delta\vartheta_i = \pi$ and black pixels correspond to $\Delta\vartheta_i = 0$ or 2π . Green trajectories correspond to pixels that are erroneously black, so they should change from $\Delta\vartheta_i = 0$ (or 2π) to $\Delta\vartheta_i = \pi$, which they do successfully. Similarly, pink trajectories correctly change from π to 0 (or 2π) while gray trajectories, corresponding to already correct pixels, do not change. For simulation details, see Sec. V.

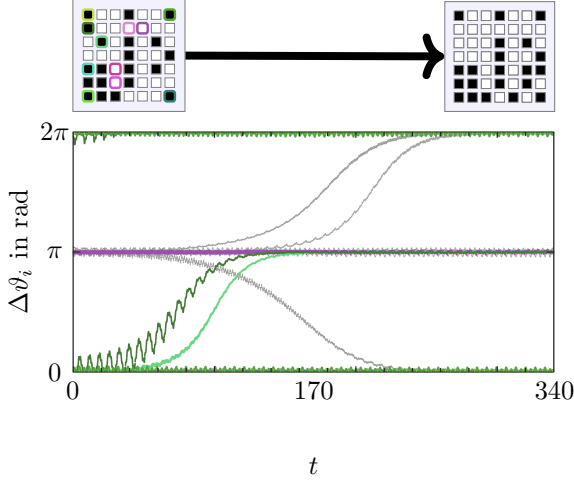


FIG. 4: Recognition fails due to too many defects: A binary pattern with 11 erroneous pixels (colored) shown on the top left should be recognized as one of 3 memorized patterns shown in Fig. 2. However, the recognition fails: Pink trajectories corresponding to pixels that are erroneously white should change from $\Delta\vartheta_i = \pi$ to $\Delta\vartheta_i = 0$ (or 2π) during the recognition process, but do not. Likewise, only 2 green trajectories change from 0 (or 2π) to $\Delta\vartheta_i = \pi$, although all 7 represent black pixels that should change to white. Additionally 3 gray trajectories, whose corresponding pixels are already correct, change to wrong values. The system settles at the pattern shown on the top right, which is none of the memorized patterns. For simulation details, see Sec. V.

connections only:

$$\begin{aligned} a^{[1/2]}(t) &= \sum_{k,l=1}^N \sum_{m=1}^M \alpha_k^m \alpha_l^m \sin \vartheta_k^{[1/2]} \sin \vartheta_l^{[1/2]} \\ &= \sum_{m=1}^M \left(\sum_{j=1}^N \alpha_j^m \sin \vartheta_j^{[1/2]} \right)^2 \end{aligned} \quad (4)$$

Whenever MONACO is used as an autoassociative memory as presented here, $a^{[1]}(t)$ and $a^{[2]}(t)$ should therefore always be constructed according to Eq. (4) instead of Eq. (1). Depending on usage, the $\bar{\alpha}^m$ can be hardwired or changed for each recognition process.

III. ANALYSIS OF THE DYNAMICS

A. Simplification of the evolution equations

Prior to determining attractors, we simplify the phase equations (Eq. (1)) with the technique of averaging [24]:

The right hand sides of Eq. (1) consist of many different frequency components. If the coupling strength ϵ is sufficiently small, larger frequencies average out on times

much smaller than the largest timescale and the smallest frequencies dominate the dynamics:

$$\begin{aligned} \dot{\vartheta}_i^{[1]} &\approx \Omega_i + \frac{\epsilon M}{8N} \sin(2\Delta\vartheta_i) \\ &\quad - \frac{\epsilon}{4N} \sum_{j=1}^N S_{ij} [\sin(\Delta\vartheta_i + \Delta\vartheta_j) + \sin(\Delta\vartheta_i - \Delta\vartheta_j)] \\ \dot{\vartheta}_i^{[2]} &\approx \Omega_i - \frac{\epsilon M}{8N} \sin(2\Delta\vartheta_i) \\ &\quad + \frac{\epsilon}{4N} \sum_{j=1}^N S_{ij} [\sin(\Delta\vartheta_i + \Delta\vartheta_j) + \sin(\Delta\vartheta_i - \Delta\vartheta_j)] \end{aligned}$$

The lengthy averaging calculation is shown in Appendix A and includes restrictions on the frequency distribution of the oscillators. Using a trigonometric theorem, we can express our equation system with the phase differences $\Delta\vartheta_i$ only:

$$\begin{aligned} \Delta\dot{\vartheta}_i &= \dot{\vartheta}_i^{[1]} - \dot{\vartheta}_i^{[2]} \approx \\ &\quad - \frac{\epsilon}{2N} \sum_{j=1}^N S_{ij} [\sin(\Delta\vartheta_i + \Delta\vartheta_j) + \sin(\Delta\vartheta_i - \Delta\vartheta_j)] \\ &\quad + \frac{\epsilon M}{4N} \sin(2\Delta\vartheta_i) \\ \Delta\dot{\vartheta}_i &= -\frac{\epsilon}{N} \sin \Delta\vartheta_i \left(\sum_{j=1}^N S_{ij} \cos \Delta\vartheta_j - \frac{M}{2} \cos \Delta\vartheta_i \right) \end{aligned} \quad (5)$$

This is the main evolution equation that governs the dynamics of the architecture.

B. Fixed points and their stability

At fixed points $\Delta\vec{\vartheta}^*$ of the dynamics, all velocity components $\Delta\dot{\vartheta}_i$ must vanish. Depending on which factor in Eq. (5) vanishes, pixel indices can be sorted into two sets p and q :

$$\begin{aligned} \bullet \quad i \in p &\Leftrightarrow \sin \Delta\vartheta_i^* = 0 \Leftrightarrow \Delta\vartheta_i^* \in \{0, \pi\} + 2\pi n \\ \bullet \quad i \in q &\Leftrightarrow \sum_{j=1}^N S_{ij} \cos \Delta\vartheta_j^* - \frac{M}{2} \cos \Delta\vartheta_i^* = 0 \end{aligned} \quad (6)$$

We show in Appendix B that all fixed points with indices in q are unstable. Therefore, all attractors are well-separated fixed points with $i \in p \forall i$.

Only fixed points with $\sin \Delta\vartheta_i^* = 0 \forall i$ and $\sum_{j=1}^N S_{ij} \cos \Delta\vartheta_j^* - M/2 \cos \Delta\vartheta_i^* \neq 0$ remain as candidates for attractors.

The stability of fixed points can generally be examined by linearizing the dynamics around the fixed point by evaluating the eigenvalues of the Jacobian $J_{ik} =$

$\partial\Delta\vartheta_i/\partial\Delta\vartheta_k$ at the fixed point $\Delta\vec{\vartheta}^*$:

$$J_{ik} = -\frac{\epsilon}{N} \cos \Delta\vartheta_i \delta_{ik} \left(\sum_{j=1}^N S_{ij} \cos \Delta\vartheta_j - \frac{M}{2} \cos \Delta\vartheta_i \right) - \frac{\epsilon}{N} \sin \Delta\vartheta_i \left(-S_{ik} \sin \Delta\vartheta_k + \frac{M}{2} \delta_{ik} \sin \Delta\vartheta_i \right)$$

As $i \in p \forall i$ implies $\sin \Delta\vartheta_i^* = 0 \forall i$, the second term vanishes:

$$J_{ik}(\Delta\vec{\vartheta}^*) = -\delta_{ik} \frac{\epsilon}{N} \cos \Delta\vartheta_i^* \left(\sum_{j=1}^N S_{ij} \cos \Delta\vartheta_j^* - \frac{M}{2} \cos \Delta\vartheta_i^* \right)$$

\mathbf{J} is a diagonal matrix, therefore eigenvectors \hat{e}_i are the standard base with the following eigenvalues:

$$\lambda_i = -\frac{\epsilon}{N} \cos \Delta\vartheta_i^* \left(\sum_{j=1}^N S_{ij} \cos \Delta\vartheta_j^* - \frac{M}{2} \cos \Delta\vartheta_i^* \right)$$

We can simplify the analysis further by defining "pattern coordinates" $\vec{\alpha}$ with $\alpha_i = \cos \Delta\vartheta_i$ as generalization of Eq. (3) and inserting the definition of the coupling matrix \mathbf{S} :

$$\begin{aligned} \lambda_i &= -\frac{\epsilon}{N} \left(\sum_{m=1}^M \alpha_i^m \alpha_i^* \sum_{j=1}^N \alpha_j^m \alpha_j^* - \frac{M}{2} \alpha_i^{*2} \right) \\ \lambda_i &= -\frac{\epsilon}{N} \left(\sum_{m=1}^M \alpha_i^m \alpha_i^* \langle \vec{\alpha}^m, \vec{\alpha}^* \rangle - \frac{M}{2} \right) \end{aligned} \quad (7)$$

The signs of the eigenvalues determine the stability: Positive eigenvalues denote growing perturbations along the corresponding eigendirection, while negative eigenvalues indicate decay. Therefore, all fixed points with $\lambda_i < 0 \forall i$ are isolated attractors:

$$\sum_{m=1}^M \alpha_i^m \alpha_i^* \langle \vec{\alpha}^m, \vec{\alpha}^* \rangle > \frac{M}{2} \quad \wedge \quad \alpha_i^* \in \{\pm 1\} \quad (8)$$

Memorized patterns map to isolated attractors, if inter-pattern scalar products are sufficiently small. If patterns $\vec{\alpha}^m$ are orthogonal, inter-pattern scalar products vanish completely:

$$\begin{aligned} \lambda_i(\vec{\alpha}^{m'}) &= -\frac{\epsilon}{N} \left(\sum_{m=1}^M \alpha_i^m \alpha_i^{m'} \langle \vec{\alpha}^m, \vec{\alpha}^{m'} \rangle - \frac{M}{2} \right) \\ &= -\frac{\epsilon}{N} \left(\sum_{m=1}^M \alpha_i^m \alpha_i^{m'} \delta_{mm'} N - \frac{M}{2} \right) \\ &= -\epsilon \left(1 - \frac{M}{2N} \right) < 0 \quad \forall i \\ \Leftrightarrow \quad M &< 2N \end{aligned} \quad (9)$$

Not more than N orthogonal patterns can exist ($\text{span}(\vec{\alpha}^m) \leq N$, but $\text{span}(\vec{\alpha}^m) = M$ for linear independent patterns.), so $M < 2N$ is always fulfilled and orthogonal patterns are guaranteed to be stable.

For general $\vec{\alpha}^m$, we get

$$\begin{aligned} \lambda_i(\vec{\alpha}^{m'}) &\stackrel{!}{<} 0 \\ -\epsilon - \frac{\epsilon}{N} \left(\sum_{m \neq m'}^M \alpha_i^m \alpha_i^{m'} \langle \vec{\alpha}^m, \vec{\alpha}^{m'} \rangle - \frac{M}{2} \right) &< 0 \\ -\sum_{m \neq m'}^M \alpha_i^m \alpha_i^{m'} \langle \vec{\alpha}^m, \vec{\alpha}^{m'} \rangle &< N - \frac{M}{2}. \end{aligned}$$

As we want a criterion to ensure that all memorized patterns are attractors, we must exclude that any eigendirection of any pattern becomes unstable:

$$\begin{aligned} \max_{i, m'} \left(-\sum_{m \neq m'}^M \alpha_i^m \alpha_i^{m'} \langle \vec{\alpha}^m, \vec{\alpha}^{m'} \rangle \right) &< N - \frac{M}{2} \\ \Sigma_{\max} \stackrel{!}{=} \max_{m'} \left(\sum_{m \neq m'}^M \left| \langle \vec{\alpha}^m, \vec{\alpha}^{m'} \rangle \right| \right) &< N - \frac{M}{2} \end{aligned} \quad (10)$$

Additionally, if the $\vec{\alpha}^m$ are attractors, their *inverses will be attractors as well* because their eigenvalues are identical:

$$\begin{aligned} \lambda_i(-\vec{\alpha}^{m'}) &= -\frac{\epsilon}{N} \left[\sum_{m=1}^M \alpha_i^m (-\alpha_i^{m'}) \langle \vec{\alpha}^m, (-\vec{\alpha}^{m'}) \rangle - \frac{M}{2} \right] \\ &= -\frac{\epsilon}{N} \left(\sum_{m=1}^M \alpha_i^m \alpha_i^{m'} \langle \vec{\alpha}^m, \vec{\alpha}^{m'} \rangle - \frac{M}{2} \right) \\ &= \lambda_i(\vec{\alpha}^{m'}) \end{aligned}$$

Moreover, there are further spurious attractors that do not represent one of the $\vec{\alpha}^m$, but they are difficult to describe. If the initial pattern does not start in the basin of attraction of an $\vec{\alpha}^m$, the output of the system will be one of these attractors. Therefore, stability is not sufficient for recognition success and we have to derive a criterion from the basins of attraction. However, first we derive a more common criterium for the network capacity that can be compared in different network architectures.

C. Error-free capacity

The *error-free capacity* $M_{\max}(N)/N$ is a measure for the amount of memorized patterns $\vec{\alpha}^m$ that can be stored in a given network while any pattern can still be retrieved without errors. Specifically, we determine the maximum number of patterns $M_{\max}(N)$ so $P(\vec{\alpha}^{m'} \text{ is stable}) \rightarrow 1$ for $M < M_{\max}(N)$ and $P(\vec{\alpha}^{m'} \text{ is stable}) \rightarrow 0$ for $M > M_{\max}(N)$. Similar to approaches for other architectures, we derive $M_{\max}(N)$ in a probabilistic manner for random memorized patterns with $P(\alpha_i^m = +1) = P(\alpha_i^m = -1) = 0.5 \forall m, i$ in the limit $N \rightarrow \infty$.

First, we simplify the rescaled Jacobian $\tilde{\mathbf{J}} = \mathbf{J}/\epsilon$ at a memorized pattern $\vec{\alpha}^{m'}$:

$$\begin{aligned}\tilde{J}_{ik}(\vec{\alpha}^{m'}) &= -\delta_{ik} \frac{1}{N} \left(\sum_{m=1}^M \alpha_i^m \alpha_i^{m'} \sum_{j=1}^N \alpha_j^m \alpha_j^{m'} - \frac{M}{2} \alpha_i^{m'^2} \right) \\ &= -\delta_{ik} \frac{1}{N} \left(\sum_{\substack{m=1 \\ m \neq m'}}^M \alpha_i^m \alpha_i^{m'} \sum_{j=1}^N \alpha_j^m \alpha_j^{m'} + N - \frac{M}{2} \right) \\ &= -\delta_{ik} \frac{1}{N} \left(\sum_{\substack{m=1 \\ m \neq m'}}^M \sum_{\substack{j=1 \\ j \neq i}}^N \alpha_i^m \alpha_i^{m'} \alpha_j^m \alpha_j^{m'} \right. \\ &\quad \left. + (M-1) + N - \frac{M}{2} \right) \\ \tilde{\mathbf{J}}(\vec{\alpha}^{m'}) &= - \left(1 + \frac{M-2}{2N} \right) \mathbf{I} + \mathbf{D}\end{aligned}$$

Here, \mathbf{I} is the identity matrix and

$$D_{ik} = -\delta_{ik} \frac{1}{N} \sum_{\substack{m=1 \\ m \neq m'}}^M \sum_{\substack{j=1 \\ j \neq i}}^N \alpha_i^m \alpha_i^{m'} \alpha_j^m \alpha_j^{m'}.$$

As $\tilde{\mathbf{J}}$, \mathbf{I} and \mathbf{D} are diagonal,

$$\begin{aligned}\lambda_{\max}(\tilde{\mathbf{J}}) &= - \left(1 + \frac{M-2}{2N} \right) + \lambda_{\max}(\mathbf{D}) \\ &= - \left(1 + \frac{M-2}{2N} \right) + \max_i D_{ii}.\end{aligned}$$

Then, the stability condition can be expressed as function of $\max_i D_{ii}$ alone:

$$\begin{aligned}\lambda_{\max}(\mathbf{J}) &< 0 \\ \Leftrightarrow \lambda_{\max}(\tilde{\mathbf{J}}) &< 0 \\ \Leftrightarrow \max_i D_{ii} &< 1 + \frac{M-2}{2N}\end{aligned}\quad (11)$$

The following lemma concerning this largest eigenvalue $\lambda_{\max}(\mathbf{D}) = \max_i D_{ii}$ has been proven in [18] as Lemma 6 under the assumption that all pixels of all memorized patterns $\vec{\alpha}^m$ are randomly chosen with probability $P(+1) = P(-1) = 0.5$: (All occurring logarithms are natural.)

Lemma 1.

Let $x > 0$, and

$$\bar{\beta} = \limsup_{N \rightarrow \infty} \frac{M(N) \log(N)}{N}, \quad \underline{\beta} = \liminf_{N \rightarrow \infty} \frac{M(N) \log(N)}{N}.$$

If $\bar{\beta} < x^2/2$, then $P(\max_i D_{ii} \geq x) \rightarrow 0$ as $N \rightarrow \infty$.
If $\underline{\beta} > x^2/2$, then $P(\max_i D_{ii} \geq x) \rightarrow 1$ as $N \rightarrow \infty$.

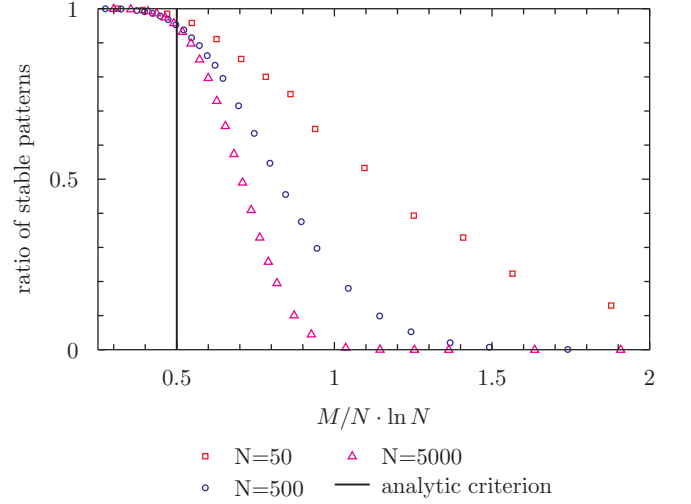


FIG. 5: The analytic criterion for the error-free capacity Eq. (12) is compared to explicit evaluation of the patterns' eigenvalues. For each datapoint, 1000 sets of pattern were created randomly with $P(\alpha_i^m = +1) = P(\alpha_i^m = -1) = 0.5$ and the stability of each pattern was determined with Eq. (8).

According to Eq. (11), $\vec{\alpha}^{m'}$ is stable for $N \rightarrow \infty$ and $M > 1$ if $\max_i D_{ii} < 1$ is fulfilled. Therefore, we are interested in the probability $P(\max_i D_{ii} \geq 1)$ and choose $x = 1$.
 $P(\vec{\alpha}^{m'} \text{ stable}) = 1 - P(\max_i D_{ii} \geq 1) \rightarrow 1$ if $\bar{\beta} < 1/2$ and $P(\vec{\alpha}^{m'} \text{ unstable}) = P(\max_i D_{ii} \geq 1) \rightarrow 1$ if $\underline{\beta} > 1/2$, which implies

$$\begin{aligned}M_{\max}(N) &= \frac{N}{2 \log(N)} \\ \Leftrightarrow \frac{M_{\max}(N)}{N} &= \frac{1}{2 \log(N)}\end{aligned}\quad (12)$$

Note that other capacity measures exist, such as the *loading rate*, which describes the fraction M_{\max}/N under the assumption that attractors for each pattern do exist, but might be shifted, so retrieved patterns might have some errors. Therefore, the *error-free capacity* always is a lower bound in the loading rate. While these probabilistic measures are useful for comparing architectures, their validity is constrained in reality: Real networks are of finite size and memorized patterns need not be chosen randomly. Bounds on guaranteed stability were derived in Eq. (10) and a criterion for guaranteed recognition is derived in Section IV.

D. Intuitive explanation of the recognition mechanism

The results of the fixed point analysis allow a more intuitive view of Eq. (5) by partially expressing the system

state in pattern coordinates $\vec{\alpha}$ with $\alpha_i = \cos \Delta\vartheta_i$:

$$\begin{aligned}\Delta\dot{\vartheta}_i &= -\frac{\epsilon}{N} \sin \Delta\vartheta_i \left(\sum_{j=1}^N S_{ij} \cos \Delta\vartheta_j - \frac{M}{2} \cos \Delta\vartheta_i \right) \\ &= -\frac{\epsilon}{N} \sin \Delta\vartheta_i \left(\sum_{j=1}^N \sum_{m=1}^M \alpha_i^m \alpha_j^m \alpha_j - \frac{M}{2} \alpha_i \right) \\ &= -\sin \Delta\vartheta_i \cdot \frac{\epsilon}{N} \left(\sum_{m=1}^M \alpha_i^m \langle \vec{\alpha}^m, \vec{\alpha} \rangle - \frac{M}{2} \alpha_i \right)\end{aligned}$$

Let $\vec{\alpha}^{m'}$ be the memorized pattern the system state $\vec{\alpha}$ is closest to:

$$\begin{aligned}\Delta\dot{\vartheta}_i &= -\sin \Delta\vartheta_i \cdot \alpha_i^{m'} \cdot \frac{\epsilon}{N} \cdot \\ &\cdot \left(\langle \vec{\alpha}^{m'}, \vec{\alpha} \rangle + \sum_{\substack{m=1 \\ m \neq m'}}^M \alpha_i^{m'} \alpha_i^m \langle \vec{\alpha}^m, \vec{\alpha} \rangle - \frac{M}{2} \alpha_i^{m'} \alpha_i \right)\end{aligned}$$

Now assume the system state $\vec{\alpha}$ is sufficiently close to $\vec{\alpha}^{m'}$: Then $\langle \vec{\alpha}^{m'}, \vec{\alpha} \rangle$ is larger than the sum of all other terms in parentheses. Hence, the fixed points and their stability are the same as in $d/dt \Delta\vartheta_i = -\alpha_i^{m'} \sin \Delta\vartheta_i$. If $\alpha_i^{m'} = +1$, $\Delta\vartheta_i^* = 0$ is stable and $\Delta\vartheta_i^* = \pi$ is unstable and vice-versa for $\alpha_i^{m'} = -1$, so $\lim_{t \rightarrow \infty} \alpha_i = \cos \Delta\vartheta_i^* = \alpha_i^{m'}$.

From another point of view, the system "defines" "relative closeness" to memorized patterns by comparing their projections onto the system state $\vec{\alpha}$. This fails, however, if the scalar products are of comparable size: Then the distribution of the α_i^m matters for each pixel, which leads to spurious attractors unequal to all $\vec{\alpha}^m$. Note that the $-M\alpha_i/2$ -term does not really contribute to the recognition mechanism. While it increases eigenvalues of all stable fixed points slightly, therefore reducing stability (see Eq. (7)), it does not influence the basins of attraction much, as we will illustrate in the next section.

IV. BASINS OF ATTRACTION AND GUARANTEED RECOGNITION

We have a firm understanding of the system now and can guarantee that the chosen patterns $\vec{\alpha}^m$ are attractive. However, we cannot guarantee recognition success yet: The system state might relax to the additional unwanted attractors described by Eq. (8) or even worse, the basins of attraction of the $\vec{\alpha}^m$ might be malformed, leading to a $\vec{\alpha}^m$ whose projection on the defective pattern is not the largest.

A. Lower bound on the basins of attraction

Matching success is guaranteed if the defective starting pattern is in the basin of attraction of the correct

memorized pattern $\vec{\alpha}^{m'}$. A lower bound on the basin of attraction can be derived by proofing the following lemmata:

1. Surfaces of constant projection on the correct memorized pattern $\vec{\alpha}^{m'}$ confine the system state to larger projections if the initial projection is sufficiently large.
2. $\vec{\alpha}^{m'}$ is the only attractor inside this confined space.

As the system state cannot leave the confined space, it has to settle on $\vec{\alpha}^{m'}$ as the only attractor. Therefore, the confined space is part of $\vec{\alpha}^{m'}$'s basin of attraction.

1. Transformation to $\vec{\alpha}$ -space

For our following discussion, we will transfer the $\Delta\vec{\vartheta}_i$ -dynamics (Eq. (5)) completely into the "pattern coordinates" $\vec{\alpha}$ with $\alpha_i = \cos \Delta\vartheta_i$, which are a generalization of the mapping of the memorized patterns $\vec{\alpha}^m$.

$$\begin{aligned}\dot{\alpha}_i &= (\cos \Delta\vartheta_i) \\ &= \frac{\partial \cos \Delta\vartheta_i}{\partial \Delta\vartheta_i} \frac{\partial \Delta\vartheta_i}{\partial t} \\ &= -\sin \Delta\vartheta_i \left[-\frac{\epsilon}{N} \sin \Delta\vartheta_i \left(\sum_{j=1}^N S_{ij} \cos \Delta\vartheta_j - \frac{M}{2} \cos \Delta\vartheta_i \right) \right] \\ &= \frac{\epsilon}{N} \sin^2 \Delta\vartheta_i \left(\sum_{j=1}^N \sum_{m=1}^M \alpha_i^m \alpha_j^m \cos \Delta\vartheta_j - \frac{M}{2} \cos \Delta\vartheta_i \right) \\ &= \frac{\epsilon}{N} (1 - \cos^2 \Delta\vartheta_i) \left(\sum_{j=1}^N \sum_{m=1}^M \alpha_i^m \alpha_j^m \cos \Delta\vartheta_j - \frac{M}{2} \cos \Delta\vartheta_i \right) \\ &= \frac{\epsilon}{N} (1 - \alpha_i^2) \left(\sum_{m=1}^M \alpha_i^m \sum_{j=1}^N \alpha_j^m \alpha_j - \frac{M}{2} \alpha_i \right) \\ \dot{\alpha}_i &= \frac{\epsilon}{N} (1 - \alpha_i^2) \left(\sum_{m=1}^M \alpha_i^m \langle \vec{\alpha}^m, \vec{\alpha} \rangle - \frac{M}{2} \alpha_i \right) \quad (13)\end{aligned}$$

Note that although the mapping between $\Delta\vartheta_i$ and α_i is *not* injective, the transformation is still valid: Eq. (5) is mirror-symmetric to $0 + \pi n$ with $n \in \mathbb{N}$, so space can be divided into regions separated by $\Delta\vartheta_i = [0, \pi] + 2\pi n$ or $\Delta\vartheta_i = [\pi, 2\pi] + 2\pi n$ in every i and flow lines in each region are mapped onto the same $\vec{\alpha}$ -coordinates. As the flow across the boundaries of these hypercubes is zero, it is not necessary to consider the periodicity of the flow.

From another point of view, the ambiguity of attractors in $\Delta\vec{\theta}$ is removed in the $\vec{\alpha}$ -coordinates. As the dynamics of $\vec{\alpha}$ do not depend on the sign or periodicity of $\Delta\vec{\theta}$, it is a more natural coordinate for the autoassociative memory.

2. Confinement by hypersurfaces of constant projection

Let's consider a hypersurface of constant projection on the correct output pattern $\vec{\alpha}^{m'}$: In the pattern coordinates the equation $\langle \vec{\alpha}, \vec{\alpha}^{m'} \rangle = C$ describes a hyperplane that divides the N -dimensional hypercube of all possible patterns into patterns with a projection larger or smaller than C . If projections on $\vec{\alpha}^{m'}$ do not decrease for all points on the surface, the system state can only move tangential to the hyperplane or towards larger projections. (Movement tangential to the hyperplane is in fact impossible with a slightly stricter condition, as shown further below.)

$$\begin{aligned} \frac{d}{dt} \frac{1}{|\vec{\alpha}^{m'}|} \langle \vec{\alpha}, \vec{\alpha}^{m'} \rangle &\geq 0 \\ \frac{d}{dt} \langle \vec{\alpha}, \vec{\alpha}^{m'} \rangle &= \langle \dot{\vec{\alpha}}, \vec{\alpha}^{m'} \rangle \geq 0 \\ \sum_{i=1}^N (1 - \alpha_i^2) \alpha_i^{m'} \left(\sum_{m=1}^M \alpha_i^m \langle \vec{\alpha}^m, \vec{\alpha} \rangle - \frac{M}{2} \alpha_i \right) &\geq 0 \quad (14) \end{aligned}$$

If Eq. (14) is fulfilled for all $\vec{\alpha}$ on a hypersurface $\langle \vec{\alpha}, \vec{\alpha}^{m'} \rangle = C$, it confines the system state. However, to exclude additional attractors besides $\vec{\alpha}^{m'}$ in the confined space is difficult with Eq. (14) and a good criterion for guaranteed recognition should neither depend on the hyperplanes nor on the specific pixels of $\vec{\alpha}$ or the memorized patterns $\vec{\alpha}^m$. Therefore, we employ a series of *worst-case approximations and upper bounds*:

Eq. (14) is fulfilled if all single summands are greater than zero. Note that this approximation also excludes movement tangential to the hypersurfaces: Without the possibility for summands to cancel each other, $d/dt \langle \vec{\alpha}, \vec{\alpha}^{m'} \rangle = 0$ is only fulfilled if $\dot{\vec{\alpha}} = 0$, so all remaining solutions are fixed points. Then the following inequalities must hold $\forall i$ and $\forall \vec{\alpha}$ on the surface:

$$\begin{aligned} \underbrace{(1 - \alpha_i^2)}_{\geq 0} \alpha_i^{m'} \left(\sum_{m=1}^M \alpha_i^m \langle \vec{\alpha}^m, \vec{\alpha} \rangle - \frac{M}{2} \alpha_i \right) &\geq 0 \\ \alpha_i^{m'} \sum_{m=1}^M \alpha_i^m \langle \vec{\alpha}, \vec{\alpha}^m \rangle - \frac{M}{2} \alpha_i^{m'} \alpha_i &\geq 0 \end{aligned}$$

$$\langle \vec{\alpha}, \vec{\alpha}^{m'} \rangle \geq - \sum_{\substack{m=1 \\ m \neq m'}}^M \alpha_i^m \alpha_i^{m'} \langle \vec{\alpha}, \vec{\alpha}^m \rangle + \frac{M}{2} \alpha_i^{m'} \alpha_i$$

As the left hand side is constant on a hypersurface, the criterion needs to be evaluated for a maximized right

hand side only and the criterion for the surface can be reduced to one single inequality:

$$\langle \vec{\alpha}, \vec{\alpha}^{m'} \rangle \geq \max_{i, \vec{\alpha}} \left(- \sum_{\substack{m=1 \\ m \neq m'}}^M \alpha_i^m \alpha_i^{m'} \langle \vec{\alpha}, \vec{\alpha}^m \rangle + \frac{M}{2} \alpha_i^{m'} \alpha_i \right)$$

The sum is maximal in i for $\alpha_i^m = -\alpha_i^{m'} \text{sgn}(\langle \vec{\alpha}, \vec{\alpha}^m \rangle) \forall m \neq m'$, as all scalar products add up. (If such an i always exists is not relevant here, as we look for a worst case approximation independent of the $\vec{\alpha}^m$.) The second term is generally much smaller, but $M/2$ at most:

$$\begin{aligned} \max_{i, \vec{\alpha}} \left(- \sum_{\substack{m=1 \\ m \neq m'}}^M \alpha_i^m \alpha_i^{m'} \langle \vec{\alpha}, \vec{\alpha}^m \rangle + \frac{M}{2} \alpha_i^{m'} \alpha_i \right) \\ \leq \max_{\vec{\alpha}} \left(\sum_{\substack{m=1 \\ m \neq m'}}^M |\langle \vec{\alpha}, \vec{\alpha}^m \rangle| + \frac{M}{2} \right) \end{aligned}$$

As the maximum of one single $|\langle \vec{\alpha}, \vec{\alpha}^m \rangle|$ is much easier to calculate, we approximate an upper bound:

$$\begin{aligned} \max_{\vec{\alpha}} \left(\sum_{\substack{m=1 \\ m \neq m'}}^M |\langle \vec{\alpha}, \vec{\alpha}^m \rangle| + \frac{M}{2} \right) \\ \leq \sum_{\substack{m=1 \\ m \neq m'}}^M \max_{\vec{\alpha}} (|\langle \vec{\alpha}, \vec{\alpha}^m \rangle|) + \frac{M}{2} \end{aligned}$$

In total, our criterion on the hypersurface has reduced to

$$C = \langle \vec{\alpha}, \vec{\alpha}^{m'} \rangle \geq \sum_{\substack{m=1 \\ m \neq m'}}^M \max_{\vec{\alpha}} (|\langle \vec{\alpha}, \vec{\alpha}^m \rangle|) + \frac{M}{2}. \quad (15)$$

While any hyperplane that fulfills Eq. (15) confines the system state to larger projections, it is still not trivial to evaluate due to the direct dependence on $\vec{\alpha}$.

3. Removing direct dependence on $\vec{\alpha}$

$\max_{\vec{\alpha}} (|\langle \vec{\alpha}, \vec{\alpha}^m \rangle|)$ can be approximated as a function of $\langle \vec{\alpha}, \vec{\alpha}^{m'} \rangle = C$ and inter-pattern scalar products.

First, $\langle \vec{\alpha}, \vec{\alpha}^{m'} \rangle$ is expressed with the difference vector $\Delta\vec{\alpha} = \vec{\alpha} - \vec{\alpha}^{m'}$ between $\vec{\alpha}$ and the closest memorized pattern $\vec{\alpha}^{m'}$:

$$\begin{aligned} \langle \vec{\alpha}, \vec{\alpha}^{m'} \rangle &= \langle \vec{\alpha} - \vec{\alpha}^{m'}, \vec{\alpha}^{m'} \rangle + \langle \vec{\alpha}^{m'}, \vec{\alpha}^{m'} \rangle \\ &= \langle \Delta\vec{\alpha}, \vec{\alpha}^{m'} \rangle + N \\ &= \sum_{i=1}^N \Delta\alpha_i \alpha_i^{m'} + N \end{aligned}$$

With $\text{sgn}(\Delta\alpha_i) = \text{sgn}(\underbrace{\alpha_i^{m'}(\alpha_i^{m'} - 1)}_{\leq 1}) = -\alpha_i^{m'}$ we get:

$$\langle \vec{\alpha}, \vec{\alpha}^{m'} \rangle = N - \sum_{i=1}^N |\Delta\alpha_i| \quad (16)$$

$$\begin{aligned} \Rightarrow \max_{\vec{\alpha}} (|\langle \vec{\alpha}, \vec{\alpha}^{m'} \rangle|) &= \max_{\Delta\vec{\alpha}} (|\langle \Delta\vec{\alpha}, \vec{\alpha}^{m'} \rangle + \langle \vec{\alpha}^{m'}, \vec{\alpha}^{m'} \rangle|) \\ &< \max_{\Delta\vec{\alpha}} \left(\sum_i \Delta\alpha_i \alpha_i^{m'} \right) + |\langle \vec{\alpha}^{m'}, \vec{\alpha}^{m'} \rangle| \\ &= \sum_i |\Delta\alpha_i| + |\langle \vec{\alpha}^{m'}, \vec{\alpha}^{m'} \rangle| \\ &= N - \langle \vec{\alpha}, \vec{\alpha}^{m'} \rangle + |\langle \vec{\alpha}^{m'}, \vec{\alpha}^{m'} \rangle| \end{aligned}$$

4. Volumes of growing projection

Finally, we can remove all direct dependence on $\vec{\alpha}$ from Eq. (15):

$$\begin{aligned} \langle \vec{\alpha}, \vec{\alpha}^{m'} \rangle &\geq \sum_{\substack{m=1 \\ m \neq m'}}^M \max_{\vec{\alpha}} (|\langle \vec{\alpha}, \vec{\alpha}^m \rangle|) + \frac{M}{2} \\ \langle \vec{\alpha}, \vec{\alpha}^{m'} \rangle &\geq \sum_{\substack{m=1 \\ m \neq m'}}^M \left(N - \langle \vec{\alpha}, \vec{\alpha}^{m'} \rangle + |\langle \vec{\alpha}^{m'}, \vec{\alpha}^m \rangle| \right) + \frac{M}{2} \\ M \cdot \langle \vec{\alpha}, \vec{\alpha}^{m'} \rangle &\geq (M-1) \cdot N + \sum_{\substack{m=1 \\ m \neq m'}}^M |\langle \vec{\alpha}^{m'}, \vec{\alpha}^m \rangle| + \frac{M}{2} \\ \langle \vec{\alpha}, \vec{\alpha}^{m'} \rangle &\geq \frac{M-1}{M} \cdot N + \frac{1}{M} \sum_{\substack{m=1 \\ m \neq m'}}^M |\langle \vec{\alpha}^{m'}, \vec{\alpha}^m \rangle| + \frac{1}{2} \quad (17) \end{aligned}$$

This final criterion for a confining hyperplane does not depend on a point on the surface.

Additionally, every surface $\langle \vec{\alpha}, \vec{\alpha}^{m'} \rangle = C_{\min}$ that fulfills Eq. (17) defines a *volume of growing projection* for larger C : As the right hand side of Eq. (17) is constant, all hyperplanes with $C > C_{\min}$ fulfill the criterion as well.

If several attractors existed in the confined space, however, no conclusion could be made on the basins of attraction, as a confined system state could move to any of them. Therefore, we exclude that any attractor besides $\vec{\alpha}^{m'}$ exists in a volume of growing projection:

5. $\vec{\alpha}^{m'}$ being the only attractor enclosed

Assume an attractor $\vec{\alpha}^a$ exists inside the region defined by Eq. (17). Now consider a small perturbation around $\vec{\alpha}^a$ that increases $\langle \vec{\alpha}, \vec{\alpha}^{m'} \rangle$, for example $\epsilon \alpha_i^{m'} \cdot \hat{e}_i$

if $\alpha_i^a \neq \alpha_i^{m'}$. As $d/dt \langle \vec{\alpha}, \vec{\alpha}^{m'} \rangle \geq 0$ in the confined space, the system cannot relax back to $\vec{\alpha}^a$. No non-isolated attractor exists (see Sec. III), so $\vec{\alpha}^a$ has at least one unstable eigendirection which contradicts the assumption that $\vec{\alpha}^a$ is an attractor.

The only exception is the attractor $\vec{\alpha}^{m'}$ itself: As it has the largest projection on itself, all perturbations must lower $\langle \vec{\alpha}, \vec{\alpha}^{m'} \rangle$.

Summing up: Every system state $\vec{\alpha}$ that obeys Eq. (17) must be in the basin of attraction of $\vec{\alpha}^{m'}$, as projection on $\vec{\alpha}^{m'}$ increases monotonically along the trajectory and $\vec{\alpha}^{m'}$ is the only attractor for larger projections.

B. Guaranteed recognition

1. Recognition criteria

As any defective initialized pattern is binary, it can be characterized by the number of defective pixels n^f in which defective input pattern and correct memorized pattern are different. Eq. (17) can be solved for n^f with Eq. (16), as n^f is a special case of $\sum_i |\Delta\alpha_i|/2$:

$$\begin{aligned} N - 2n^f &> \frac{M-1}{M} \cdot N + \frac{1}{M} \sum_{\substack{m=1 \\ m \neq m'}}^M |\langle \vec{\alpha}^{m'}, \vec{\alpha}^m \rangle| + \frac{1}{2} \\ n^f &< \frac{1}{2M} \left(N - \sum_{\substack{m=1 \\ m \neq m'}}^M |\langle \vec{\alpha}^{m'}, \vec{\alpha}^m \rangle| \right) - \frac{1}{4} \quad (18) \end{aligned}$$

(The equality in Eq. (17) must be dropped here, as perturbations and higher order terms neglected in Eq. (5) might push a defective pattern on the outermost hyperplane out of the confined space.)

For *pairwise orthogonal patterns*, $\langle \vec{\alpha}^{m'}, \vec{\alpha}^m \rangle = 0 \forall m \neq m'$ and Eq. (18) becomes:

$$\boxed{n^f < \frac{N}{2M} - \frac{1}{4}} \quad (19)$$

We now treat *general patterns* with $\langle \vec{\alpha}^{m'}, \vec{\alpha}^m \rangle \neq 0$. A criterion that does not depend on the correct memorized pattern $\vec{\alpha}^{m'}$ is obtained with the definition $\Sigma_{\max} = \max_{\vec{\alpha}^{\tilde{m}}} (\sum_{m=1, m \neq \tilde{m}}^M |\langle \vec{\alpha}^{\tilde{m}}, \vec{\alpha}^m \rangle|) > \sum_{m=1, m \neq m'}^M |\langle \vec{\alpha}^{m'}, \vec{\alpha}^m \rangle|$ from Sec. III. Then the worst case of Eq. (18) is

$$\boxed{n^f < \frac{N - \Sigma_{\max}}{2M} - \frac{1}{4}} \quad (20)$$

Eq. (20) guarantees successful recognition for arbitrary patterns.

2. Consistency Check

The basin of attraction has to vanish when the fixed point loses stability. Therefore, we can regain stability criteria for the $\vec{\alpha}^m$ by minimizing the necessary extension of the basin of attraction in Eq. (19) and Eq. (20), which corresponds to $\lim_{n^f \rightarrow 0}$:

$$\lim_{n^f \rightarrow 0} \text{Eq. (19)} : \quad 0 < \frac{N}{2M} - \frac{1}{4} \\ M < 2N$$

This coincides with our calculation that pairwise orthogonal patterns are always stable: At most, N orthogonal patterns can exist, as they are linear independent and $\dim(\text{span}(\{\vec{\alpha}^m\})) \leq N$, so $M < 2N$ is always fulfilled.

$$\lim_{n^f \rightarrow 0} \text{Eq. (20)} : \quad 0 < \frac{N - \Sigma_{max}}{2M} - \frac{1}{4} \\ \Sigma_{max} < N - \frac{M}{2}$$

This again reproduces our result for the stability of non-orthogonal patterns.

V. NUMERICAL SIMULATIONS

In this section we validate our criterion for successful pattern recognition with simulations of the full phase dynamics Eq. (1).

A. Numerical methods and parameters

The equations have been implemented in C and integration was performed with the classical Runge-Kutta method. A timestep $dt = 1 \cdot 10^{-4}$ and a coupling strength $\epsilon = 0.1$ were used. The angular frequencies were distributed according to $\Omega_i = 1200 + 1800 \cdot G_i/G_N$, where G_i is the i -th element of a Golomb ruler [25] (see also Appendix A). The near optimal Golomb rulers used were both taken from [26]: $\{0, 17, 20, 86, 119, 140, 166, 227, 240, 255, 353, 430, 520, 559, 564, 565, 602, 675, 724, 781, 817, 833, 905, 929, 961, 970, 980, 1131, 1162, 1189, 1212, 1319, 1403, 1433, 1437, 1451, 1462, 1497, 1504, 1589, 1601, 1680, 1763, 1785, 1825, 1880, 1888, 1956, 1958\}$ for $N = 49$ and $\{0, 34, 44, 91, 95, 147, 207, 278, 332, 364, 375, 405, 458, 520, 682, 698, 701, 710, 853, 868, 901, 946, 973, 1022, 1080, 1150, 1155, 1172, 1240, 1254, 1290, 1429, 1540, 1546, 1605, 1642, 1682, 1684, 1705, 1751, 1771, 1806, 1835, 1943, 1967, 2041, 2151, 2164, 2182, 2189, 2190, 2270\}$ for $N = 52$.

For simulations in Fig. 3 and Fig. 4, defective patterns were chosen manually and memorized patterns are taken from Fig. 2. All pseudorandom numbers (necessary for random distribution of erroneous pixels and construction of random orthogonal patterns) were created using C's

n^f	6-11	12	13	14	15	16
failed recognitions ♥	0	0	0	1	5	13
failed recognitions ♠	0	2	2	3	3	15
failed recognitions π	0	1	2	6	6	22
failure rate	0%	0.3%	0.4%	1.1%	1.6%	5.6%

TABLE I: Failed Recognitions with non-orthogonal patterns as shown in Fig. 2. 300 recognitions were performed for each pattern and each number of erroneous pixels n^f . Erroneous pixels were distributed randomly for each simulation.

standard random number generator `rand()` from `stdlib`, which was seeded with the time in microseconds times the process ID.

B. Testing criteria for guaranteed recognition

In order to test criteria Eq. (19) and (20), simulations were performed for both the non-orthogonal patterns shown in Fig. 2 with $N=49$ pixels as well as for 3 random orthogonal patterns with $N=52$ pixels. Simulations started after setting the initial conditions to a defective pattern similar to one of the memorized patterns but different in exactly n^f randomly distributed erroneous pixels. In order to save simulation time, simulations were aborted if the system state reached one of the memorized patterns, as they are proven to be attractors. In all other cases, simulations were continued until $|\alpha_i| \geq 0.9 \forall i$ for a period $t_{wait} = 500$. Recognition success was tested by projecting the $\vec{\alpha}$ -coordinates of the final system state on the memorized patterns: If $\langle \vec{\alpha}, \vec{\alpha}^{m'} \rangle / N > 0.99$, recognitions were counted as successful.

For the non-orthogonal patterns with $M = 3$, $N = 49$ and $\Sigma_{max} = 10$, the recognition criterion Eq. (20) predicts recognition success for $n^f < (N - \Sigma_{max}) / (2M) - 0.25 = 6.25$. 300 simulations were performed for $n^f \in \{6..16\}$ for each pattern and results are summed up in Table I. All recognitions were successful for $n^f \leq 11$ and the rate of failed recognitions grows slowly for larger n^f . Obviously, our criterion seems to be too strict.

Similarly, 1000 simulations were performed with orthogonal random patterns with $N = 52$ and $M = 3$ for each $n^f \in \{8..17\}$. Here, $n^f < N / (2M) - 0.25 = 8.42$ is predicted by Eq. (19). Random orthogonal patterns were constructed by using the elementwise product \circ : As orthogonal patterns with $\alpha_i \in \pm 1$ differ in exactly $N/2$ pixels, a pattern $\vec{\alpha}^2$ orthogonal to any pattern $\vec{\alpha}^1$ can be easily found by creating a "difference vector" $\vec{d}^{1,2}$, where $N/2 + 1$ - and -1 -entries are randomly distributed. Then $\vec{\alpha}^2 = \vec{\alpha}^1 \circ \vec{d}^{1,2}$.

For 3 orthogonal patterns, $\vec{\alpha}^1$, $\vec{d}^{1,2}$ and $\vec{d}^{1,3}$ were first chosen randomly. Then $|\langle \vec{\alpha}^2, \vec{\alpha}^3 \rangle| = |\langle \vec{d}^{1,2}, \vec{d}^{1,3} \rangle|$ was minimized by switching 2 randomly selected pixels in a randomly selected difference vector, if the absolute value

n^f	8-12	13	14	15	16	17
failed recognitions	0	1	1	4	13	29
failure rate	0%	0.1%	0.1%	0.4%	1.3%	2.9%

TABLE II: Failed Recognitions with random orthogonal patterns with $N = 52$ pixels. 1000 recognitions were performed for each number of erroneous pixels n^f . Random distribution of erroneous pixels and the construction of random orthogonal patterns was repeated for each simulation.

of the scalar product diminished.

Results are summed up in Table II. Similar to the simulations with non-orthogonal patterns, recognitions are always successful for $n^f \leq 12$, which is significantly larger than predicted by the criterion for guaranteed recognition. For even larger n^f , the rate of failed recognitions stays small.

C. Failed recognitions are rare events

One might expect that the criterion for guaranteed recognition is not optimal for both the orthogonal random patterns and our choice of non-orthogonal patterns, so that 7 respectively 9 erroneous pixels or even more can always be correctly recognized as well. However, failed recognitions are just rare for $n^f = 7$ / $n^f = 9$ instead. We now construct problematic starting patterns with $n^f = 7$ for the non-orthogonal memorized patterns that fail in the recognition process:

According to Eq. (15), recognition will fail if the scalar products between the defective starting pattern and non-similar memorized patterns are extremized. Considering the scalar products $\langle \vec{\alpha}^\heartsuit, \vec{\alpha}^\pi \rangle = +5$, $\langle \vec{\alpha}^\heartsuit, \vec{\alpha}^\clubsuit \rangle = -5$, and $\langle \vec{\alpha}^\pi, \vec{\alpha}^\clubsuit \rangle = -1$, an erroneous heart-pattern is most likely to fail. Assume furthermore that the number of erroneous pixels n^f is fixed. Then the right hand side of Eq. (15) can be maximized by distributing the errors on positions where they increase the projection on the π - and decrease the projection on the \clubsuit -pattern. 10 such "worst-case" positions can be found for the \heartsuit -pattern and $\binom{10}{7} = 120$ possible combinations exist to distribute $n^f = 7$ erroneous pixels on the "worst-case" positions.

Simulations were performed for all of these "worst case patterns". Recognition failed for all simulations and the system state relaxed to an attractor with projections of 0.59, -0.51 and 0.51 on the \heartsuit -, \clubsuit - and π -pattern. Possible worst-case positions for erroneous pixels and the irregular output pattern are shown in Fig. 6. Indeed, simulations with randomly distributed errors could not recognize this: As there are $\binom{49}{7} \approx 8,6 \cdot 10^7$ possibilities to distribute the erroneous pixel on the pattern and only $\binom{10}{7} = 120$ worst case distributions can be found, the chance to encounter a failing random starting pattern is almost negligible. Furthermore, all $\binom{10}{6} = 210$ worst-case-patterns for $n^f = 6$ were successfully recognized as

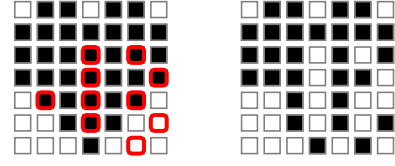


FIG. 6: On the left side, an unperturbed \heartsuit -pattern is shown. Erroneous pixels on red-circled positions extremize the sum of inter-pattern scalar products. All erroneous \heartsuit -patterns with 7 erroneous pixels on marked locations fail the recognition process. Simulations of all such patterns resulted in the spurious attractor shown on the right.

the \heartsuit -pattern in simulations, which again validates Eq. (20) as criterion for guaranteed recognition. Similar calculations can be performed for the orthogonal case. This is a good example that extracting basins of attractions in high-dimensional systems with simulations can only give an approximation on the success rate but no guaranteed criterion. From another point of view, failed recognitions are rare, so a higher n^f is acceptable if a non-perfect recognition rate is sufficient.

VI. DISCUSSION

MONACO gains its distinctive properties from two design features:

1. *Two mirrored globally coupled subnetworks* are used.

First of all, the use of two groups enables the internal generation of the coupling modulations. Second, the effective coordinates of the network are phase differences $\Delta\vartheta_i$ of oscillators of equal frequency. Values of phase differences can easily be read out by multiplying signals of an oscillator pair and using a low-pass filter, gaining $\cos\Delta\vartheta_i$. Similarly, setting the initial conditions requires only positive or negative coupling between two oscillators forming a pair. Third, the effective average coupling strength ϵ is doubled with two subnetworks, enabling faster recognition (compare with Appendix A). The fourth advantage is much subtle: In all architectures with externally generated coupling modulations, frequencies in the coupling modulation are fixed to the natural frequencies of the uncoupled oscillators. However, the so-called "acceleration effect" [27] changes the frequencies of even weakly coupled oscillators. Any mismatches between oscillator frequency and coupling modulation frequency components would further limit the coupling strength ϵ . As a higher coupling strength reduces recognition time, we decided to avoid the problem altogether: Since oscillators in both networks are affected symmetrically by the coupling, the acceleration effect will be equal and frequen-

cies in the coupling modulations are adjusted automatically. It is noteworthy, that the coupling between single oscillator pairs is above the Kuramoto threshold and thus frequencies of the two oscillators adapt. Hence, the architecture allows for some tolerance in the frequency mismatch of an oscillator pair.

2. Novel *coupling modulations* are used.

As shown in Eq. (4), the used coupling modulations can be constructed with $\mathcal{O}(N \cdot M)$ connections only. Note that there cannot be any better scaling, as patterns consist of $N \cdot M$ independent pixels. Additionally, this coupling modulations introduce novel effective dynamics Eq. (5), where the only existing attractors are isolated fixed points with $\cos \Delta\vartheta_i \in \{\pm 1\}$ (Section III). As every pixel settles at these binary values, the output is inherently digital, which further simplifies readout and subsequent processing. All memorized patterns are attractive if inter-pattern scalar products are not too large (see Eq. (10) for guaranteed stability). As memorized patterns are no transient phenomenon, but long-term stable, readout does not need to be exactly timed and the output can be retrieved at a later time. Furthermore, the dynamics allow us to calculate a lower bound on the basins of attraction analytically (Section IV). This leads to a non-probabilistic criterion for guaranteed recognition that includes finite-size effects, Eq. (20).

Note that the mirrored subnetwork structure should not be confused with "layers" from "traditional" layered neural networks. MONACO is very similar to a continuous version of the Hopfield model[10] (compare with Eq. (13)): Each oscillator pair corresponds to an artificial neuron that "stores" its phase difference $\Delta\vartheta_i$. The synchronization process can be seen as continuous updating of the $\Delta\vartheta_i$. MONACO's subnetworks, however, change the properties of the "neurons", while the ideal effective dynamics Eq. (5) remain unchanged except for the coordinates they are represented in. This is distinct from more "traditional" layered neural networks, where the layer structure is essential to the dynamics.

On the contrary, a design with two subnetworks is not necessary in order to obtain the described dynamics including isolated attractors: A multiplicative coupling modulation suffices; consider e.g. the following single-network-system:

$$\dot{\vartheta}_i = \Omega_i + \cos \vartheta_i \cdot a_{ext}(t) \cdot \frac{\epsilon}{N} \sum_{j=1}^N \sin \vartheta_j$$

$$a_{ext}(t) = \sum_{k,l=1}^N S_{kl} \sin \Omega_k t \sin \Omega_l t$$

Here, the averaged dynamics would be the same as for MONACO, but in coordinates $\varphi_i(t) = \vartheta_i(t) - \Omega_i t$ (com-

pare with Appendix A):

$$\dot{\varphi}_i = -\frac{\epsilon}{2N} \left(\sum_{j=1}^N S_{ij} \sin \varphi_i \cos \varphi_j - \frac{M}{2} \sin \varphi_i \cos \varphi_i \right)$$

Phase shifts φ_i must be used, as no oscillators with equal frequencies exist in this setup and therefore, phase differences $\Delta\vartheta_i$ are no useful coordinate. As discussed below, tracking changes of the φ_i requires very precise frequency and time measurements, which renders readout difficult and error-prone. Therefore, this exemplary network is inferior to MONACO.

The MONACO-architecture will now be compared to other associative memories consisting of phase oscillators. Distinctive features are compared in Table III, while schematics of are shown in Fig. 7.

We discriminate between two types of networks: In *physically* all-to-all connected networks (architectures (I)[12–14] and (III)[18]), oscillators have the same frequencies and every oscillator is connected with every other (see Fig. 7 a). Therefore, the number of connections scales with $\mathcal{O}(N^2)$ in these networks, which limits the networks' size. As proposed in [15], oscillators of different frequency can be all-to-all connected *dynamically* with only one physical connection per oscillator if the oscillators' coupling is modulated in time. In architecture (IIA)[15, 16], the oscillators are globally coupled to a sum of the oscillators' signals with a single temporal modulation of the coupling (see Fig. 7 b). Due to the global coupling, the number of connections scales with $\mathcal{O}(N)$ connections only.

Architecture (IIB)[15, 17] follows a slightly more complicated scheme, where every oscillator receives the signals of all other oscillators, but each oscillator has its own coupling modulation (see Fig. 7 c). Nevertheless, the scaling of the number of connections is still $\mathcal{O}(N)$.

MONACO is a dynamically all-to-all connected network as well. Each subnetwork is globally coupled similar to (IIA), albeit with a different coupling modulation (see Fig. 1). The use of two mirrored subnetworks allows for the *internal* generation of the global coupling modulations. In contrast, the hardware implementation for architectures (IIA) and (IIB) introduced in [16, 17] was fed by computer-generated coupling modulations. In MONACO, the scaling of the number of connections is $\mathcal{O}(N \cdot M)$ (see Eq. 4 for the coupling modulations and consider that global coupling scales with $\mathcal{O}(N)$). This scaling is optimal if the generation of the coupling modulations is considered, as $N \cdot M$ pixels have to be incorporated.

However, the reduction in the number of spatial connections is not for free: The original complexity in space is transferred to a complexity in time with the number of frequencies contained in the coupling modulation growing like $\mathcal{O}(N^2)$ for architecture (IIA) and MONACO[15]. Frequency conditions for architecture (IIB) are less restrictive and the number of frequencies scales with $\mathcal{O}(N^{\ln 3 / \ln 2})$ [17].

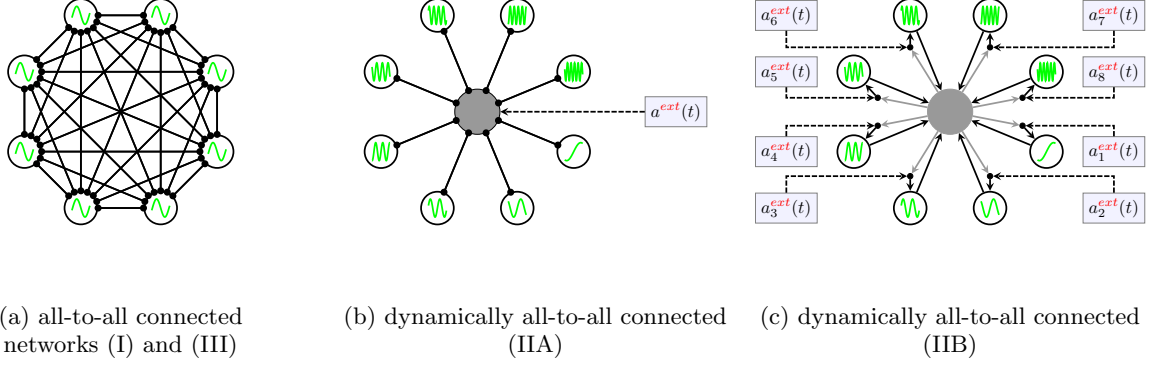


FIG. 7: Schematics of previous oscillatory neural network architectures that act as autoassociative memories

network property	all-to-all connected network (I) [12–14]	dynamically all-to- all connected (IIA) [15, 16]	dynamically all-to- all connected (IIB) [15, 17]	all-to-all connected with higher order fourier modes (III) [18]	MONACO
Number of connections	$\mathcal{O}(N^2)$	$\mathcal{O}(N) + \text{external}$ coupling modulation $\geq \mathcal{O}(N \cdot M)$	$\mathcal{O}(N) + \text{external}$ coupling modulation $\geq \mathcal{O}(N \cdot M)$	$\geq \mathcal{O}(N^2)$; coupling function implemen- tation unknown	$\mathcal{O}(N \cdot M)$
frequency distribution	$\mathcal{O}(N^0)$	$\mathcal{O}(N^2)$	$\mathcal{O}(N^{\ln 3 / \ln 2})$	$\mathcal{O}(N^0)$	$\mathcal{O}(N^2)$
initialization quality	ambiguous, fast	ambiguous[29], slow	ambiguous[29], slow	ambiguous, fast	not ambiguous, fast
effective recognition dynamics	$\dot{\vartheta}_i - \Omega =$ $\epsilon \sum_{j=1}^N S_{ij} \sin(\vartheta_j - \vartheta_i)$	$\dot{\varphi}_i =$ $\epsilon \sum_{j=1}^N S_{ij} \sin(\varphi_j - \varphi_i)$	$\dot{\varphi}_i =$ $\epsilon \sum_{j=1}^N S_{ij} \sin(\varphi_j - \varphi_i)$	$\dot{\vartheta}_i - \Omega = 1/N \left(\sum_{j=1}^N S_{ij} \sin(\vartheta_j - \vartheta_i) + \bar{\epsilon} \sin 2(\vartheta_j - \vartheta_i) \right)$	$\Delta \dot{\vartheta}_i = -\epsilon/N \left(\sum_{j=1}^N S_{ij} \sin \Delta \vartheta_i \cos \Delta \vartheta_j - \frac{M}{2} \sin \Delta \vartheta_i \cos \Delta \vartheta_i \right)$
isolated at- tractors?	\times [21]			✓	✓
loading rate	≤ 0.048 [31–33]			$\geq \frac{2\epsilon^2}{\log N}$	$\geq \frac{1}{2 \log N}$
error-free capacity	$\frac{2}{N}$ [12, 18]			$\frac{2\epsilon^2}{\log N}$	$\frac{1}{2 \log N}$

TABLE III: Comparison of MONACO with other autoassociative memory architectures based on phase-oscillator networks. The best performances for every property are marked in green.

Now, coordinates of the network dynamics will be discussed, as they determine how initial conditions can be enforced as well as how the system state can be read out. In (I) and (III), the desired dynamics occur in oscillators' phases $\vartheta_i = \Omega t + \varphi_i$, so pixels of the same value have the same phase. An encoded pattern is then represented by two groups of oscillators whose phases differ by π . Note that this representation itself is ambiguous, as it is physically impossible to decide if a group follows or precedes the other one. In other words, the physical state represents a pattern as well as its inverse. In (IIA) and (IIB), equal pixels are represented by equal phase shifts φ_i and different pixels differ by a phase shift difference

of π . Note that phase shifts are only unique up to a constant $\varphi_i^0 = \varphi_i(t=0)$. As a consequence, only differences $\varphi_i(t) - \varphi_i(t')$ can be determined. In MONACO patterns are coded into phase differences $\Delta \vartheta_i = \vartheta_i^{[1]} - \vartheta_i^{[2]}$ of oscillators of equal frequencies. Each pixel is mapped onto a phase difference with $\alpha_i = \cos \Delta \vartheta_i$, so $\alpha_i = +1$ corresponds to a synchronized oscillator pair and $\alpha_i = -1$ to an antisynchronized one. Therefore, MONACO's system state represents a pattern without ambiguity.

The different nature of the variables entail that also the setting of initial conditions differs radically between architectures: Phase differences in MONACO are easily manipulatable: Oscillator pairs corresponding to +1 are

directly coupled positively, while pixels with -1 receive a negative coupling, resulting in synchronized pairs with $\Delta\vartheta_i = 0$ or $\Delta\vartheta_i = \pi$. Phases ϑ_i change quickly in time, so they are difficult to control directly. However, initial conditions in (I) and (III) can be set similar to MONACO by coupling all N oscillators in a row, where oscillators representing equal pixels are coupled positively and unequal pixels interact via a negative coupling. In (IIA) and (IIB), two main problems must be overcome to set initial conditions: First, phase shifts cannot be manipulated directly and second, phase shifts are undefined without a temporal reference. Hoppensteadt and Izhikevich[15] proposed to use the same coupling circuitry as used for the recognition, but with a different coupling matrix \mathbf{S} : $S_{ij} = \alpha_i^d \alpha_j^d$ is used to initialize a defective pattern $\vec{\alpha}^d$. Then, recognition is performed with the usual coupling matrix $S_{ij} = \sum_{m=1}^M \alpha_i^m \alpha_j^m$. By evaluating phase shift changes between the introduced initial condition and the recognition, pixel changes can be retrieved without the constants φ_i^0 . However, initialized patterns are ambiguous: As $S_{ij}(-\vec{\alpha}^d) = (-1)^2 \alpha_i^d \alpha_j^d = S_{ij}(\vec{\alpha}^d)$, the inverse pattern $-\vec{\alpha}^d$ is initialized half of the time. Additionally, as this method is limited by the averaging condition similar to the recognition, this method is of timescale $1/\epsilon$ and therefore considerably slower than the direct coupling used for (I), (III) and MONACO.

Similarly, readout of the final pattern is easy in MONACO: As mentioned above, $\cos \Delta\vartheta_i = \alpha_i$ can be read out directly from the corresponding oscillator pair. Readout in (I) and (III) is analogue, but phase differences between different pixels are determined, which again describes both a specific pattern and its inverse. For (IIA) and (IIB), phase shifts have to be determined by comparing the phase of an oscillator with an external reference. Then, the difference of phase shifts between final state and the initial conditions needs to be evaluated. In refs. [16, 17], this was done with a computer and analog-digital converter cards [28, 29].

Ease of readout additionally depends on the effective dynamics of the architectures: Traditional Kuramoto-type networks (I) employ a coupling that depends only on the mutual phase differences of all oscillators ($\propto \sin(\vartheta_i - \vartheta_j)$). While (IIA) and (IIB) have a seemingly more complex structure due to their coupling modulations, dynamics are effectively the same as in (I) after averaging (Compare with Table III), albeit in different coordinates. In these dynamics, the individual patterns are not individual attractors, but part of one large attractor. More precisely, patterns are connected by lines of attractive non-isolated fixed points[21]. Consequently, recognition is only possible for short times, as the system state drifts on the attractor due to implementation inaccuracies and higher order terms and readout must occur immediately after the recognition is successful. Additionally, the system state does only settle close to the correct memorized pattern, so the output values are not inherently digital as the patterns are.

MONACO's dynamics (cf. Eq. (1)) take on a simple mathematical form after averaging (Eq. (5) for the formulation in phase differences, Eq. (13) in pattern space $\vec{\alpha}$). In these novel dynamics, binary memorized patterns are *individual* attractors. In [18], yet another dynamics was introduced with architecture (III) (see Table III). Memorized patterns are isolated attractors here as well due to higher order Fourier modes in the coupling function. Due to the isolated attractors, readout does not need to be exactly timed and the output is inherently digital in MONACO as well as in architecture (III). Additionally, the dynamics of (III) enable the exclusion of spurious attractors for specific parameter ranges, while MONACO's dynamics allowed us to determine lower bounds on the basins of attraction, as discussed below and in Section IV.

Concerning quantitative measures for associative networks, often the capacity or loading rate of a network is used. It describes the maximum possible ratio of M and N , where the system state still settles close to the correct memorized pattern. Usually, it is computed for a set of random memorized patterns in the limit $N \rightarrow \infty$. This definition, however, includes deviations from the memorized patterns, so e.g. some bits may be erroneous at retrieval. Nishikawa et al. point out the importance of error-free retrieval for engineering applications [18] and remind of the error-free capacity (def. in Subsec. III C) as a more meaningful quantity, as it is used for traditional neural networks [30]. The error-free capacity of MONACO (Eq. (12)) is on a par with architecture (III)[18] and equal to the error-free capacity of the Hopfield model [30] while memorized patterns are typically unstable in architectures (I), (IIA) and (IIB) with an error-free capacity of $2/N$ [12, 18]. The loading rate for architectures (I),(IIA) and (IIB) has been derived as 0.048 [31–33], while it has not been calculated for neither architecture (III) nor MONACO yet. However, the error-free capacities are lower bounds on the loading rates and may be larger than the value for (I) - (IIB) similar to the error-free capacities.

While the loading rate and the error-free capacity are useful for comparing architectures, their probabilistic nature and the derivation for $\lim N \rightarrow \infty$ impair their significance for real networks: Specific sets of memorized patterns are possibly not random and finite size effects might improve or impair pattern stability as well as recognition success. Non-probabilistic criteria valid for all network sizes allow to exactly evaluate performance of a network for a specific use case and enable the development of more complex algorithms using the recognition process repeatedly. We derived such criteria for MONACO: Eq. (10) guarantees stability of all memorized patterns if scalar products between memorized patterns are not too large. Eq. (20) guarantees recognition success by giving a lower bound on the number of allowed erroneous pixels n^f . If a network stores a large number of patterns M , the minimal size of the basins of attraction will be quite small and few erroneous pixels n^f can be

guaranteed to be corrected. In many applications, however, the number of patterns M is much smaller than N and the ability to correct larger errors is desired.

The last aspects to be discussed concern recognition time and oscillator accuracy. In physically all-to-all connected networks (I) and (III), oscillator frequencies are not restrictive, as long as they are similar enough to be well above the Kuramoto transition. In contrast, frequency conditions in dynamically all-to-all connected networks limit the network size: Since in practice there will be only a certain frequency interval available, the number of oscillators is limited by the accuracy of the frequencies [16]. Recognition times have not been calculated analytically for any of the oscillatory neural networks presented here. However, we assume that the frequency restrictions present in (IIA), (IIB) and MONACO lead to slower recognition times compared to (I) or (III). Nevertheless, the shift of frequency due to the acceleration effect [27] present in the real dynamics of (IIA) and (IIB) [15, 16, 21] does not interfere with the recognition process in MONACO since the change in frequency is identical in each oscillator pair due to its mirrored structure. Additionally, it is likely that the introduction of several coupling modulations per subnetwork similar to the transition from architecture (IIA) to (IIB) is possible for the MONACO-architecture. In this improved network the scaling of necessary frequencies would be reduced to $\mathcal{O}(N^{\ln(3)/\ln(2)})$.

VII. SUMMARY & OUTLOOK

We presented a network of coupled nonlinear oscillators as a new architecture for an autoassociative memory device. Two subnetworks of oscillators with equal frequency distributions are each globally coupled. An additional temporal modulation of the coupling is constructed from signals of oscillators in the other subnetwork and the binary memorized patterns. The oscillator pairs of equal frequency synchronize to phase shifts of either 0 or π , which corresponds to the pixel values of a binary output pattern. Furthermore, the number of connections scales linearly with the number of pixels N and the only necessary input are defective pattern and memorized patterns. While orthogonal memorized patterns are always attractors, general memorized patterns are stable as well if their projections on each other are not too large. Although spurious attractors also exist, we derived a simple criterion for guaranteed recognition from worst case approximations on the basins of attraction for orthogonal as well as general patterns. Finally, our results were confirmed by simulations, which also indicate that failed recognitions might occur but are quite rare as long as the criterion for guaranteed recognition is only weakly missed. While other oscillatory neural networks exist which scale linearly with the number of pixels N or have isolated attractors, our MONACO-architecture is the first to combine both features as well as the first

to provide solid criteria for guaranteed recognition.

Several questions remain open: The first concerns the maximal possible value of ϵ since a large ϵ decreases recognition time. Additionally, the system's robustness to frequency deviations or noise has not been quantified yet and might be addressed both theoretically or experimentally. In principle, a hardware realization is independent of the exact type of oscillator as long as their signal shape is close to harmonic. Thus, also fast state-of-the-art nano-oscillators [34, 35] are conceivable. In this context, the influence of small delays should be discussed.

Finally, an even better time-connection tradeoff might be possible: Distributing frequency components on multiple coupling modulations similar to [17] might provide better scaling of recognition time combined with all the other benefits of our architecture.

ACKNOWLEDGMENTS

We want to thank Alexander Sparber and Stefan Litzel for fruitful discussions and careful reading. Furthermore, we thank the Nanosystems Initiative Munich (NIM) for financial support.

Appendix A: Averaging and frequency restrictions

In this Appendix, we apply the method of averaging [24] to the phase description Eq. 1. Therefore, we first expand the products in Eq. (1) with the trigonometric equalities $\sin x \cos y = [\sin(x - y) + \sin(x + y)]/2$ and $\sin x \sin y = [\cos(x - y) - \cos(x + y)]/2$ to obtain all frequency components:

$$\begin{aligned}
 \dot{\vartheta}_i^{[1]} - \Omega_i &= \\
 &= \frac{\epsilon}{N} \cos \vartheta_i^{[1]} \cdot \sum_{j=1}^N a^{[2]}(t) \sin \vartheta_j^{[1]} \\
 &= \frac{\epsilon}{N} \sum_{j,k,l=1}^N S_{lk} \sin \vartheta_l^{[2]} \cos \vartheta_i^{[1]} \cdot \sin \vartheta_j^{[1]} \sin \vartheta_k^{[2]} \\
 &= \frac{\epsilon}{4N} \sum_{j,k,l=1}^N S_{lk} \left[\sin(\vartheta_l^{[2]} - \vartheta_i^{[1]}) + \sin(\vartheta_l^{[2]} + \vartheta_i^{[1]}) \right] \\
 &\quad \cdot \left[\cos(\vartheta_j^{[1]} - \vartheta_k^{[2]}) - \cos(\vartheta_j^{[1]} + \vartheta_k^{[2]}) \right] \\
 &= \frac{\epsilon}{8N} \sum_{j,k,l=1}^N S_{lk} \left[\begin{aligned} &\sin(\vartheta_l^{[2]} - \vartheta_i^{[1]} - \vartheta_j^{[1]} + \vartheta_k^{[2]}) \\ &+ \sin(\vartheta_l^{[2]} - \vartheta_i^{[1]} + \vartheta_j^{[1]} - \vartheta_k^{[2]}) \\ &- \sin(\vartheta_l^{[2]} - \vartheta_i^{[1]} - \vartheta_j^{[1]} - \vartheta_k^{[2]}) \\ &- \sin(\vartheta_l^{[2]} - \vartheta_i^{[1]} + \vartheta_j^{[1]} + \vartheta_k^{[2]}) \\ &+ \sin(\vartheta_l^{[2]} + \vartheta_i^{[1]} - \vartheta_j^{[1]} + \vartheta_k^{[2]}) \\ &+ \sin(\vartheta_l^{[2]} + \vartheta_i^{[1]} + \vartheta_j^{[1]} - \vartheta_k^{[2]}) \\ &- \sin(\vartheta_l^{[2]} + \vartheta_i^{[1]} - \vartheta_j^{[1]} - \vartheta_k^{[2]}) \\ &- \sin(\vartheta_l^{[2]} + \vartheta_i^{[1]} + \vartheta_j^{[1]} + \vartheta_k^{[2]}) \end{aligned} \right]
 \end{aligned}$$

As $\vartheta_i^{[1/2]} = \Omega_i t + \mathcal{O}(\epsilon)$, each of the sin-terms might oscillate with frequencies of $\mathcal{O}(\Omega_i)$ or $\mathcal{O}(\Delta\Omega_{ij})$. ($\Delta\Omega_{ij} =$

$\Omega_i - \Omega_j$) As the characteristic timescales $\mathcal{O}(\Omega_i^{-1})$ and $\mathcal{O}(\Delta\Omega_{ij}^{-1})$ are much smaller than ϵ^{-1} , the time average of these oscillating terms vanishes on times $\mathcal{O}(\epsilon^{-1}) \gg \mathcal{O}(\Delta\Omega_{ij}^{-1})$. If frequencies in the argument cancel each other out, however, the argument is constant on timescales $\mathcal{O}(\epsilon^{-1})$ and all oscillating terms are negligible. Depending on the signs in the sin-argument, there can be different possibilities how constant terms can arise:

In the first term, for example, frequencies cancel if $\Omega_l + \Omega_k = \Omega_i + \Omega_j$. That is always true for $l = i \wedge k = j$ or $l = j \wedge k = i$, imposing an interaction between the i -th and j -th oscillators in both networks depending on S_{ij} . However, frequencies might also cancel if the frequency distribution is chosen poorly, which would wrongly connect oscillators with different numbers i, j, k, l only dependent on S_{lk} . Therefore, we require $\Omega_l + \Omega_k \neq \Omega_m + \Omega_n \forall$ pairwise different l, k, m, n .

Similarly, the lowest order is obtained in the third term for $\Omega_l = \Omega_i + \Omega_j + \Omega_k$. In order to avoid interaction between the i -th and j -th oscillators based on S_{lk} again, the frequency distribution must obey $\Omega_l \neq \Omega_m + \Omega_n + \Omega_k \forall l, k, m, n$ and the third term becomes negligible as well as the fourth, fifth and sixth term.

While the eighth term averages out without further conditions, we get identical contributions from the second and the seventh term. This can be seen by renaming indices l and k and using $S_{lk} = S_{kl}$:

$$\begin{aligned} \dot{\vartheta}_i^{[1]} - \Omega_i &\approx \\ &\approx \frac{\epsilon}{8N} \sum_{j,k,l=1}^N S_{lk} \left[\right. \\ &\quad (\delta_{il}\delta_{kj} + \delta_{ik}\delta_{lj} - \delta_{ik}\delta_{kl}\delta_{lj}) \sin(\vartheta_l^{[2]} - \vartheta_i^{[1]} - \vartheta_j^{[1]} + \vartheta_k^{[2]}) \\ &\quad \left. + 2\delta_{il}\delta_{kj} \sin(\vartheta_l^{[2]} - \vartheta_i^{[1]} + \vartheta_j^{[1]} - \vartheta_k^{[2]}) \right] \\ &= \frac{\epsilon}{8N} \sum_{j=1}^N \left[-S_{ij} \sin((\vartheta_i^{[1]} - \vartheta_i^{[2]}) + (\vartheta_j^{[1]} - \vartheta_j^{[2]})) \right. \\ &\quad - S_{ji} \sin((\vartheta_i^{[1]} - \vartheta_i^{[2]}) + (\vartheta_j^{[1]} - \vartheta_j^{[2]})) \\ &\quad + 2S_{ij} \sin((\vartheta_i^{[1]} - \vartheta_i^{[2]}) - (\vartheta_j^{[1]} - \vartheta_j^{[2]})) \left. \right] \\ &\quad + \frac{\epsilon}{8N} S_{ii} \sin(2(\vartheta_i^{[1]} - \vartheta_i^{[2]})) \end{aligned}$$

Final simplifications can be obtained by introducing the phase difference of oscillators with identical frequency $\Delta\vartheta_i = \vartheta_i^{[1]} - \vartheta_i^{[2]}$ and using $S_{ji} = S_{ij}$ as well as $S_{ii} = M$. For $\dot{\vartheta}_i^{[2]}$, the calculation is the same with inverted upper indices:

$$\begin{aligned} \dot{\vartheta}_i^{[1]} &= \Omega_i + \frac{\epsilon M}{8N} \sin(2\Delta\vartheta_i) \\ &\quad - \frac{\epsilon}{4N} \sum_{j=1}^N S_{ij} [\sin(\Delta\vartheta_i + \Delta\vartheta_j) + \sin(\Delta\vartheta_i - \Delta\vartheta_j)] \end{aligned}$$

$$\begin{aligned} \dot{\vartheta}_i^{[2]} &= \Omega_i - \frac{\epsilon M}{8N} \sin(2\Delta\vartheta_i) \\ &\quad + \frac{\epsilon}{4N} \sum_{j=1}^N S_{ij} [\sin(\Delta\vartheta_i + \Delta\vartheta_j) + \sin(\Delta\vartheta_i - \Delta\vartheta_j)] \end{aligned}$$

Remark:

As shown in [16], both conditions on the frequency distribution can be simplified further: (l, k, m, n are still pairwise different.)

$$\begin{aligned} \Omega_l + \Omega_k &\neq \Omega_m + \Omega_n \\ \Omega_l - \Omega_n &\neq \Omega_m - \Omega_k \\ \Delta\Omega_{ln} &\neq \Delta\Omega_{mk} \end{aligned}$$

All difference frequencies have to be different to each other. This can be fulfilled by multiplying the minimal difference frequency $\Delta\Omega_{min}$ with a Golomb-ruler [25], a set of integers with non-equal differences. Similarly, the second condition can be simplified to $\Omega_l - \Omega_m = \Delta\Omega_{lm} \neq \Omega_n + \Omega_k \forall l, k, m, n$. This last inequality is always fulfilled if $\Omega_{min} > \Omega_{max}/3$.

Appendix B: Ljapunov function and unstable fixed point sets

In this Appendix, we derive a Ljapunov function for Eq. (5). We use it to show that all fixed points with at least one index i that fulfills Eq. 6 are unstable.

1. Ljapunov function

First, we express Eq. (5) as a gradient system with potential U , where $\Delta\dot{\vartheta}_i = -\partial U / \partial \Delta\vartheta_i \forall i$:

$$U = -\frac{\epsilon}{2N} \sum_{l=1}^N \left(\sum_{k=1}^N S_{kl} \cos \Delta\vartheta_k \cos \Delta\vartheta_l - \frac{M}{2} \cos^2 \Delta\vartheta_l \right)$$

This is equivalent to the overdamped motion of a particle in an energy landscape, where $\vec{v} \propto -\vec{\nabla} E$. Therefore, U decreases along trajectories and is a Ljapunov-function, which ensures that fixed points are the only attractors possible in Eq. (5).

2. unstable fixed points

In order to prove that all fixed points with some $i \in q$ are unstable, we express the system state in pattern coordinates $\vec{\alpha}$ with $\alpha_i = \cos \Delta\vartheta_i$ and insert the coupling matrix $S_{ij} = \sum_{m=1}^M \alpha_i^m \alpha_j^m$ into our potential function U :

$$U = -\frac{\epsilon}{2N} \sum_{l=1}^N \left(\sum_{k=1}^N S_{kl} \cos \Delta\vartheta_k \cos \Delta\vartheta_l - \frac{M}{2} \cos^2 \Delta\vartheta_l \right)$$

$$\begin{aligned}
&= -\frac{\epsilon}{2N} \sum_{k,l=1}^N \left(\sum_{m=1}^M \alpha_k^m \alpha_l^m \alpha_k \alpha_l - \frac{M}{2} \delta_{kl} \alpha_l^2 \right) \\
&= -\frac{\epsilon}{2N} \left(\sum_{m=1}^M \langle \vec{\alpha}^m, \vec{\alpha} \rangle^2 - \frac{M}{2} \langle \vec{\alpha}, \vec{\alpha} \rangle \right)
\end{aligned}$$

Now consider a small perturbation $\gamma \hat{e}_i$ from a fixed point $\vec{\alpha}^*$ where $i \in q$:

$$\begin{aligned}
U(\vec{\alpha}^* + \gamma \hat{e}_i) &= \\
&= -\frac{\epsilon}{2N} \left[\sum_{m=1}^M \left(\langle \vec{\alpha}^m, \vec{\alpha}^* \rangle + \underbrace{\langle \vec{\alpha}^m, \gamma \hat{e}_i \rangle}_{=\gamma \alpha_i^m} \right)^2 - \frac{M}{2} \langle \vec{\alpha}^*, \vec{\alpha}^* \rangle \right. \\
&\quad \left. + 2 \langle \vec{\alpha}^*, \gamma \hat{e}_i \rangle + \langle \gamma \hat{e}_i, \gamma \hat{e}_i \rangle \right]
\end{aligned}$$

$$\begin{aligned}
&= U(\vec{\alpha}^*) - \frac{\epsilon \gamma}{N} \underbrace{\left(\sum_{m=1}^M \alpha_i^m \langle \vec{\alpha}^m, \vec{\alpha}^* \rangle - \frac{M}{2} \alpha_i^* \right)}_{=0, \text{ as } i \in q. (\text{see Eq. (6)})} \\
&\quad - \frac{\epsilon}{2N} \left(\sum_{m=1}^M \gamma^2 \underbrace{(\alpha_i^m)^2}_{=+1} - \frac{M}{2} \gamma^2 \right) \\
&= U(\vec{\alpha}^*) - \frac{\epsilon M}{4N} \gamma^2
\end{aligned}$$

As U decreases close to $\vec{\alpha}^*$, there must be an unstable eigendirection and the fixed point must be unstable if at least one i with $\sum_{j=1}^N S_{ij} \cos \Delta \vartheta_j^* - \frac{M}{2} \cos \Delta \vartheta_i^* = 0$ exists. (i.e. $i \in q$)

Therefore, only the isolated fixed points with $\sin \Delta \vartheta_i^* = 0 \forall i$ and $S_{ik} \sin \Delta \vartheta_k^* - M/2 \delta_{ik} \sin \Delta \vartheta_i^* \neq 0 \forall i$ can be attractors.

-
- [1] Arkady Pikovsky, Michael Rosenblum, and Jürgen Kurths, *Synchronization: a universal concept in nonlinear sciences*, Vol. 12 (Cambridge university press, 2003).
 - [2] Grigory V Osipov, Jürgen Kurths, and Changsong Zhou, *Synchronization in oscillatory networks* (Springer Science & Business Media, 2007).
 - [3] Susanna C Manrubia, Alexander S Mikhailov, *et al.*, *Emergence of dynamical order: synchronization phenomena in complex systems*, Vol. 2 (World Scientific, 2004).
 - [4] Stefano Boccaletti, *The synchronized dynamics of complex systems*, Vol. 6 (Elsevier, 2008).
 - [5] Andrzej Stefański, *Determining Thresholds of Complete Synchronization and Application*, Vol. 67 (World Scientific, 2009).
 - [6] Takashi Nishikawa, ed., *Synchronization and Cascading Processes in Complex Networks [Focus Issue]*, Vol. 21 (AIP Publishing, 2011).
 - [7] Johan AK Suykens and Grigory V Osipov, *Synchronization in complex networks [Focus Issue]*, Vol. 18 (AIP Publishing, 2008).
 - [8] Juergen Kurths, Stefano Boccaletti, Celso Grebogi, and Ying-Cheng Lai, eds., *Control and synchronization in chaotic dynamical systems [Focus Issue]*, Vol. 13 (AIP Publishing, 2003).
 - [9] Frank C Hoppensteadt and Eugene M Izhikevich, *Weakly connected neural networks*, Vol. 126 (Springer Science & Business Media, 2012).
 - [10] John J Hopfield, “Neural networks and physical systems with emergent collective computational abilities,” *Proceedings of the National Academy of Sciences* **79**, 2554–2558 (1982), <http://www.pnas.org/content/79/8/2554.full.pdf>.
 - [11] Juan A. Acebrón, Luis L. Bonilla, Conrad J. Pérez Vicente, Félix Ritort, and Renato Spigler, “The kuramoto model: A simple paradigm for synchronization phenomena,” *Rev. Mod. Phys.* **77**, 137–185 (2005).
 - [12] Toru Aonishi, “Phase transitions of an oscillator neural network with a standard hebb learning rule,” *Physical Review E* **58**, 4865 (1998).
 - [13] Toshio Aoyagi and Katsunori Kitano, “Effect of random synaptic dilution in oscillator neural networks,” *Physical Review E* **55**, 7424 (1997).
 - [14] Alex Arenas and Conrad J Pérez Vicente, “Exact long-time behavior of a network of phase oscillators under random fields,” *Physical review E* **50**, 949 (1994).
 - [15] Frank C. Hoppensteadt and Eugene M. Izhikevich, “Oscillatory neurocomputers with dynamic connectivity,” *Phys. Rev. Lett.* **82**, 2983–2986 (1999).
 - [16] Robert W Hölzel and Katharina Krischer, “Pattern recognition with simple oscillating circuits,” *New Journal of Physics* **13**, 073031 (2011).
 - [17] Kathrin Kistorz, Robert W Hölzel, and Katharina Krischer, “Distributed coupling complexity in a weakly coupled oscillatory network with associative properties,” *New Journal of Physics* **15**, 083010 (2013).
 - [18] Takashi Nishikawa, Frank C Hoppensteadt, and Ying-Cheng Lai, “Oscillatory associative memory network with perfect retrieval,” *Physica D: Nonlinear Phenomena* **197**, 134–148 (2004).
 - [19] Rosangela Follmann, Elbert EN Macau, Epaminondas Rosa, and Jose RC Piqueira, “Phase oscillatory network and visual pattern recognition,” *Neural Networks and Learning Systems, IEEE Transactions on* **26**, 1539–1544 (2015).
 - [20] Donald Olding Hebb, *The organization of behavior: A neuropsychological theory* (Psychology Press, 2005).
 - [21] Robert W. Hölzel and Katharina Krischer, “Stability and long term behavior of a hebbian network of kuramoto oscillators,” *SIAM Journal on Applied Dynamical Systems* **14**, 188–201 (2015), <http://dx.doi.org/10.1137/140965168>.
 - [22] Note that coupling modulations were named ”coupling

- functions” by Hölzel [16], but this term is already used differently in the field.
- [23] Yoshiaki Kuramoto, *Chemical oscillations, waves, and turbulence*, Vol. 19 (Springer Science & Business Media, 2012).
 - [24] Ferdinand Verhulst, *Nonlinear Differential Equations and Dynamical Systems*, Hochschultext / Universitext (Springer Berlin Heidelberg, 1996).
 - [25] Solomon W Golomb, “The use of combinatorial structures in communication signal design,” in *Applications of Combinatorial Mathematics*, Institute of Mathematics and its Applications Conference Series, Vol. 60 (1997) pp. 59–78.
 - [26] Mike D Atkinson and Anne-Lise Hassenklover, “Sets of integers with distinct differences,” in *Rep. SCS-TR-63* (School of Comp. Sci., Carleton Univ Ottawa, Ont., Canada, 1984).
 - [27] Toru Aonishi, Koji Kurata, and Masato Okada, “Acceleration effect of coupled oscillator systems,” *Phys. Rev. E* **65**, 046223 (2002).
 - [28] *This should in principle be possible with precise reference oscillators, a precise clock and a memory for the initialized phase shift values as well.* ().
 - [29] *As Readout in (IIA) and (IIB) only measures changes between initial values and thus the final pattern can be constructed non-ambiguously from the initial defective pattern, the ambiguity introduced in the setting of initial values is effectively removed.* ().
 - [30] Robert J McEliece, Edward C Posner, Eugene R Rodemich, and Santosh S Venkatesh, “The capacity of the hopfield associative memory,” *Information Theory, IEEE Transactions on* **33**, 461–482 (1987).
 - [31] Toshio Aoyagi and Katsunori Kitano, “Retrieval dynamics in oscillator neural networks,” *Neural computation* **10**, 1527–1546 (1998).
 - [32] J Cook, “The mean-field theory of a q-state neural network model,” *Journal of Physics A: Mathematical and General* **22**, 2057 (1989).
 - [33] Satoki Uchiyama and Hirokazu Fujisaka, “Stability of oscillatory retrieval solutions in the oscillator neural network without lyapunov functions,” *Physical Review E* **65**, 061912 (2002).
 - [34] Gyorgy Csaba and Wolfgang Porod, “Computational study of spin-torque oscillator interactions for non-boolean computing applications,” *Magnetics, IEEE Transactions on* **49**, 4447–4451 (2013).
 - [35] Thomas C Jackson, Abhishek A Sharma, James A Bain, Jeffrey A Weldon, and Lawrence Pileggi, “Oscillatory neural networks based on two nano-oscillators and multi-level rram cells,” *Emerging and Selected Topics in Circuits and Systems, IEEE Journal on* **5**, 230–241 (2015).